

2023

## Review-Electrode Kinetics and Electrolyte Stability in Vanadium Flow Batteries

Andrea Bourke

*Technological University of the Shannon, Ireland*

Daniela Oboroceanu

*Technological University Dublin, Ireland, daniela.oboroceanu@tudublin.ie*

Nathan Quill

*Department of Physics and Bernal Institute, University of Limerick, Ireland*

*See next page for additional authors*

Follow this and additional works at: <https://arrow.tudublin.ie/scschphyart>

 Part of the [Biological and Chemical Physics Commons](#), and the [Optics Commons](#)

### Recommended Citation

Bourke, Andrea; Oboroceanu, Daniela; Quill, Nathan; Lenihan, Catherine; Maria Alhajji Safi, Maria Alhajji Safi; Miller, Mallory A.; Savinell, Robert F.; Wainright, Jesse S.; SasikumarSP, Varsha; Rybalchenko, Maria; Amini, Pupak; Dalton, Niall; Lynch, Robert P; and Buckley, D. Noel, "Review-Electrode Kinetics and Electrolyte Stability in Vanadium Flow Batteries" (2023). *Articles*. 184.

<https://arrow.tudublin.ie/scschphyart/184>

This Article is brought to you for free and open access by the School of Physics, Clinical and Optometric Science at ARROW@TU Dublin. It has been accepted for inclusion in Articles by an authorized administrator of ARROW@TU Dublin. For more information, please contact [arrow.admin@tudublin.ie](mailto:arrow.admin@tudublin.ie), [aisling.coyne@tudublin.ie](mailto:aisling.coyne@tudublin.ie), [vera.kilshaw@tudublin.ie](mailto:vera.kilshaw@tudublin.ie).



This work is licensed under a [Creative Commons Attribution-Share Alike 4.0 International License](#).

---

## Authors

Andrea Bourke, Daniela Oboroceanu, Nathan Quill, Catherine Lenihan, Maria Alhajji Safi Maria Alhajji Safi, Mallory A. Miller, Robert F. Savinell, Jesse S. Wainright, Varsha SasikumarSP, Maria Rybalchenko, Pupak Amini, Niall Dalton, Robert P. Lynch, and D. Noel Buckley

**OPEN ACCESS**

## Review—Electrode Kinetics and Electrolyte Stability in Vanadium Flow Batteries

To cite this article: Andrea Bourke *et al* 2023 *J. Electrochem. Soc.* **170** 030504

View the [article online](#) for updates and enhancements.

### You may also like

- [Towards Optical Monitoring of Vanadium Redox Flow Batteries \(VRFBs\): An Investigation of the Underlying Spectroscopy](#)  
D. Noel Buckley, Xin Gao, Robert P. Lynch et al.
- [Electrochemical Pretreatment of Carbon Fibre Electrodes and Its Effect on the Kinetics of Vanadium Redox Reactions](#)  
Andrea Bourke, Mallory A. Miller, Robert P Lynch et al.
- [Electrode Kinetics of Vanadium Flow Batteries: Contrasting Responses of  \$V^{II}\$ ,  \$V^{III}\$  and  \$V^{IV}\$ - \$V^V\$  to Electrochemical Pretreatment of Carbon](#)  
A. Bourke, M. A. Miller, R. P. Lynch et al.



 **Connect with decision-makers at ECS**

Accelerate sales with ECS exhibits, sponsorships, and advertising!

▶ Learn more and engage at the 244th ECS Meeting!



## Review—Electrode Kinetics and Electrolyte Stability in Vanadium Flow Batteries

Andrea Bourke,<sup>1,2,\*</sup> Daniela Oboroceanu,<sup>1,3</sup> Nathan Quill,<sup>1,4</sup> Catherine Lenihan,<sup>1</sup> Maria Alhajji Safi,<sup>1</sup> Mallory A. Miller,<sup>5,\*</sup> Robert F. Savinell,<sup>1,6,\*\*</sup>  Jesse S. Wainright,<sup>6,\*</sup> Varsha SasikumarSP,<sup>1,2,\*\*\*</sup> Maria Rybalchenko,<sup>1,\*\*\*</sup> Pupak Amini,<sup>1</sup> Niall Dalton,<sup>1,a</sup> Robert P. Lynch,<sup>1,6,\*</sup>  and D. Noel Buckley<sup>1,6,z,\*\*</sup> 

<sup>1</sup>Department of Physics and Bernal Institute, University of Limerick, Ireland

<sup>2</sup>Department of Electrical & Electronic Engineering, Technological University of the Shannon, Ireland

<sup>3</sup>School of Physics, Clinical and Optometric Sciences, Technological University Dublin, Ireland

<sup>4</sup>Department of Physics, South East Technological University, Ireland

<sup>5</sup>Moses Lake Industries, Advanced Research Center, Portland, Oregon, United States of America

<sup>6</sup>Department of Chemical and Biomolecular Engineering, Case Western Reserve University, Cleveland, Ohio, United States of America

Two aspects of vanadium flow batteries are reviewed: electrochemical kinetics on carbon electrodes and positive electrolyte stability. There is poor agreement between reported values of kinetic parameters; however, most authors report that kinetic rates are faster for  $V^{IV}/V^V$  than for  $V^{II}/V^{III}$ . Cycling the electrode potential increases the rates of both reactions initially due to roughening but when no further roughening is observed, the  $V^{II}/V^{III}$  and  $V^{IV}/V^V$  reactions are affected oppositely by the pretreatment potential. Anodic pretreatment activates the electrode for the  $V^{II}/V^{III}$  reaction, and deactivates it for  $V^{IV}/V^V$ . Three states of the carbon surface are suggested: reduced and oxidized states R and O, respectively, both with low electrocatalytic activity, and an intermediate state M with higher activity. The role of surface functional groups and the mechanisms of electron transfer for the  $V^{II}/V^{III}$  and  $V^{IV}/V^V$  reactions are still not well understood. The induction time for precipitation of  $V_2O_5$  from positive electrolytes decreases with temperature, showing an Arrhenius-type dependence with an activation energy of 1.79 eV in agreement with DFT calculations based on a  $VO(OH)_3$  intermediate. It also decreases exponentially with increasing  $V^V$  concentration and increases exponentially with increasing sulphate concentration. Both arsenate and phosphate are effective additives for improving thermal stability.

© 2023 The Author(s). Published on behalf of The Electrochemical Society by IOP Publishing Limited. This is an open access article distributed under the terms of the Creative Commons Attribution Non-Commercial No Derivatives 4.0 License (CC BY-NC-ND, <http://creativecommons.org/licenses/by-nc-nd/4.0/>), which permits non-commercial reuse, distribution, and reproduction in any medium, provided the original work is not changed in any way and is properly cited. For permission for commercial reuse, please email: [permissions@iopublishing.org](mailto:permissions@iopublishing.org). [DOI: [10.1149/1945-7111/acbc99](https://doi.org/10.1149/1945-7111/acbc99)]



Manuscript received December 16, 2022. Published March 7, 2023. *This paper is part of the JES Focus Issue on Frontiers of Chemical/Molecular Engineering in Electrochemical Energy Technologies in Honor of Robert Savinell.*

The present shift towards renewable energy involves the rapidly increasing deployment in electricity grids of non-dispatchable power sources such as solar, wind and ocean energy.<sup>1–3</sup> Due to the intermittency of these sources, their use is restricted unless there is a means of storing the energy they produce in periods of high availability for utilization in periods of limited availability.<sup>4</sup> This has created an urgent need for large-scale electrical energy storage<sup>1,5–8</sup> to which redox flow batteries<sup>9–29</sup> offer a promising solution due to advantages over other electrical energy storage technologies.<sup>11,30</sup> Consequently, research activities in this area have grown exponentially in recent years.<sup>31,32</sup>

The energy storage capability and power output of a flow battery, unlike conventional batteries, can be scaled independently to suit the desired application.<sup>13</sup> Other advantages<sup>33</sup> include a high degree of safety, long lifetime, potentially low capital costs, high reliability and relatively high energy efficiency. Among the numerous systems that have been studied, the vanadium flow battery (VFB), also known as the vanadium redox flow battery (VRFB), is commonly regarded as one of the most promising.<sup>10,12,13,34–39</sup> The chemistry of this system is perhaps the most thoroughly characterized and the cell design has been considerably optimized.<sup>6,37,38</sup> It has seen the widest commercial deployment<sup>36</sup> and systems as large as 400 MWh have been demonstrated.<sup>40,41</sup> Compared to other flow battery systems, VFBs have the additional advantage that they are essentially immune to cross-contamination problems due to mass transfer across the

membrane that can limit the service life of the electrolyte in other systems.<sup>6,10–12,42–45</sup> This is because both the positive and negative sides of a VFB are based on vanadium species, eliminating the need for costly re-purification processes.<sup>1,46</sup> Furthermore if rebalancing<sup>47,48</sup> of the system is required the electrolytes in the two reservoirs can be mixed with each other. Since aqueous vanadium species are highly colored, the vanadium concentrations and state-of-charge of both sides of a VFB may be precisely monitored using ultraviolet-visible (UV-vis) spectroscopy.<sup>49–53</sup>

Carbon or graphite felts have been the preferred electrode type for VFBs.<sup>9,26,54–58</sup> Their self-supporting three-dimensional fibrous structure provides reasonable surface areas and low resistance to electrolyte flow.<sup>54</sup> Carbon papers,<sup>59</sup> which have long been used in fuel cell applications, are a promising alternative. Novel carbon materials<sup>26,54,60–68</sup> such as electrospun carbon nanofibers<sup>60–64</sup> are also being investigated. Usually in a VFB stack, each electrode is connected to another electrode of opposite polarity in an adjacent cell. Contact between electrodes is made by means of an electrically conducting plate, called a bipolar plate,<sup>26,54</sup> which is in contact with each of the porous electrodes and also serves as the barrier which separates the electrolytes of the adjacent half-cells. Suitable composites of carbon and a polymeric material are usually used for bipolar plates. Carbon has very good stability as long as the positive side of the flow-battery is not overcharged.<sup>69,70</sup> Typically, coulombic efficiencies of over 90%<sup>71,72</sup> are obtained in VFBs.

Active areas of research on VFBs include cell design and modelling,<sup>13,43,73</sup> performance and state-of-charge (SoC) monitoring,<sup>49–53,74–79</sup> coulombic and energy efficiencies,<sup>80,81</sup> electrolytes,<sup>78,79,82–84</sup> membranes,<sup>85–88</sup> and electrodes.<sup>16,18,70,84,89–122</sup> Clearly, this encompasses a broad spectrum of studies ranging from fundamental electrochemical processes to practical issues of engineering, materials and technology and there have been several recent

\*Electrochemical Society Member.

\*\*Electrochemical Society Fellow.

\*\*\*Electrochemical Society Student Member.

<sup>a</sup>Present address: Integrated Graphene Ltd, Euro House, Stirling, FK8 2DY, United Kingdom.

<sup>z</sup>E-mail: [noel.buckley@UL.ie](mailto:noel.buckley@UL.ie)

review and perspective publications.<sup>9,23–26,31,32</sup> In this paper, we specifically review two fundamental areas in which we work: electrochemical kinetics on carbon electrodes and electrolyte stability.

### Electrochemical Kinetics on Carbon Electrodes

**Kinetics and mechanism of the  $V^{II}/V^{III}$  and  $V^{IV}/V^V$  redox reactions.**—Among the major factors affecting the energy efficiency of a VFB are the overpotentials at the electrodes. It has been widely reported that the overpotential at the negative electrode is generally higher than that at the positive. The kinetics of the  $V^{II}/V^{III}$  and  $V^{IV}/V^V$  reactions at the negative and positive electrodes, respectively, have been investigated in experimental flow cells with both carbon felts<sup>17,123–125</sup> and carbon papers<sup>95,126,127</sup> using techniques such as electrochemical impedance spectroscopy (EIS) and chronoamperometry (CA). In some studies overpotentials have been monitored with respect to open circuit potentials at auxiliary carbon electrodes<sup>17,61,124</sup> and in other studies reference electrodes<sup>128</sup> have been incorporated into the flow cells.<sup>17,61,95,126</sup> Some typical results are listed in Table I.

It can be seen that there is a considerable variation in the data both for  $V^{II}/V^{III}$  and for  $V^{IV}/V^V$ . Such variation between studies using electrode materials from different sources with different pretreatments etc. is not unexpected. It might be expected, though, that there would be agreement, between studies, on the ratio of the corresponding values for  $V^{II}/V^{III}$  and  $V^{IV}/V^V$  measured under similar conditions within each study. However, it can be seen from Table I that such agreement is also very poor. For example, reported values of the ratio of the electrochemical rate constant for  $V^{IV}/V^V$  to that for  $V^{II}/V^{III}$  ( $r = k_0^{45}/k_0^{23}$ ) vary from 1.4 to 11.5 for carbon paper and from 1.9 to 5.3 for carbon felt. The variation among other reported values is even greater. In particular, we note large differences between values for the same electrode material after different pretreatments. For example, Choi et al.<sup>125</sup> used EIS in a symmetric flow-cell configuration to investigate the kinetics of  $V^{IV}/V^V$  and  $V^{II}/V^{III}$  on carbon felt electrodes before and after thermal pretreatment. Before pretreatment, the exchange current density was 147 times larger for  $V^{IV}/V^V$  than for  $V^{II}/V^{III}$ ; after thermal pretreatment this ratio dropped to 8.86. The pretreatment improved the kinetics of both couples but the improvement for  $V^{II}/V^{III}$  was much greater. Likewise, Mazúr et al.<sup>123</sup> reported that thermal pretreatment of carbon felt improved  $V^{II}/V^{III}$  kinetics by about an order of magnitude, but made much smaller differences to  $V^{IV}/V^V$  kinetics, while Shao-Horn and coworkers<sup>127</sup> reported that, after thermal pretreatment,  $V^{II}/V^{III}$  kinetics on carbon paper were enhanced but  $V^{IV}/V^V$  kinetics were unchanged. Possible reasons for

this strong dependence on electrode pretreatment will be discussed later.

Despite the poor agreement between actual ratios, there is general agreement among the results of flow cell studies that the kinetics are faster for  $V^{IV}/V^V$  than for  $V^{II}/V^{III}$ . For example, Zawodzinski et al.<sup>95</sup> incorporated reference electrodes into flow cells and conducted polarisation experiments in situ on carbon paper electrodes to directly compare the kinetics of the two half-cells under the same conditions. They reported that exchange current densities for the positive half-cell were 44 times larger than those for the negative half-cell. Cecchetti et al.<sup>126</sup> also incorporated reference electrodes into flow cells with carbon paper electrodes and showed higher overpotentials in the negative half-cell than in the positive half-cell. This finding was supported by EIS and CA measurements. Similarly, Becker et al.<sup>124</sup> showed higher overpotentials at carbon felt electrodes in the negative half-cell of a flow cell than in the positive half-cell by incorporating potential probes (made from carbon fibers). Their results are supported by EIS measurements where higher rate constants (5.3 times) were determined for the  $V^{IV}/V^V$  reaction than for the  $V^{II}/V^{III}$  reaction. Similar results were obtained for carbon paper by Pour et al.<sup>127</sup> and for carbon felt by Mazur et al.<sup>123</sup> Kjeang et al.<sup>97,129</sup> developed a novel microfluidic three-electrode flow cell to study the kinetic rates of  $V^{IV}/V^V$  and  $V^{II}/V^{III}$  at carbon paper under forced electrolyte flow. From CA experiments, they reported the kinetic rates of the  $V^{IV}/V^V$  reaction as being nearly two orders of magnitude larger than those for the  $V^{II}/V^{III}$  reaction. Becker et al.<sup>130</sup> also employed a three-electrode flow-cell apparatus and reported that the kinetic rates of  $V^{IV}/V^V$  were faster than those of  $V^{II}/V^{III}$  on carbon paper (1.4 times) and carbon felt (1.9 times) from CA experiments. (See Table I).

**Studies of electrode kinetics on carbon in conventional three-electrode cells.**—In efforts to better understand the electrode kinetics of the  $V^{II}/V^{III}$  and  $V^{IV}/V^V$  redox couples, various investigators have used conventional three-electrode cells and a variety of electrochemical techniques including cyclic voltammetry (CV), CA and EIS measurements. A range of different carbon materials have been studied including glassy carbon, pyrolytic graphite, carbon-polymer, graphite, carbon fibers, carbon felt, carbon paper and carbon xerogel.

Compared with the results discussed above for flow cell experiments, these three-electrode-cell studies show even greater variation in the data for  $V^{II}/V^{III}$ , for  $V^{IV}/V^V$ , and for the ratio of the two couples. Again, it is generally reported that  $V^{IV}/V^V$  kinetics are faster than  $V^{II}/V^{III}$ . In early work, Skyllas-Kazacos et al. reported,<sup>26,93,94</sup> based on CVs at glassy carbon electrodes, that the electrochemical rate constant  $k_0^{45}$  for  $V^{IV}/V^V$  was 44 times larger

**Table I. Summary of reported studies of kinetics of  $V^{II}/V^{III}$  and  $V^{IV}/V^V$  in experimental flow cells. Values of the electrochemical rate constants  $k_0$ , exchange current density  $j_0$ , or charge transfer resistance  $R_{ct}$  are shown for carbon electrodes, both felt and paper, after a variety of pretreatments. Values for both  $V^{II}/V^{III}$  and  $V^{IV}/V^V$  as well as their ratios are shown.**

Electrode Material	Pretreatment	Measurement Technique	Kinetic rate value		
			$V^{II}/V^{III}$	$V^{IV}/V^V$	Ratio
			$k_0$ ( $\times 10^{-6} \text{ cm s}^{-1}$ )		
Felt <sup>130</sup>	As received	CA	12	23	1.9
Felt <sup>124</sup>	As received	EIS	30	160	5.3
Paper <sup>130</sup>	As received	CA	1.6	2.3	1.4
Paper <sup>97</sup>	As received	CA	5.54	63.6	11.5
Paper <sup>97</sup>	Wet-proofed	CA	6.6	49	7.4
			$j_0$ ( $\text{mA cm}^{-2}$ )		
Felt <sup>125</sup>	As received	EIS	7	1027	147
Felt <sup>125</sup>	Thermal	EIS	161	1427	8.86
Paper <sup>95</sup>	As received	CA	0.149	6.48	44
Paper <sup>129</sup>	Thermal	CA	0.04	$\sim 3$	$\sim 75$
			$R_{ct}$ ( $\Omega \text{ cm}^2$ )		
Felt <sup>123</sup>	As received	EIS	1.08	0.18	6

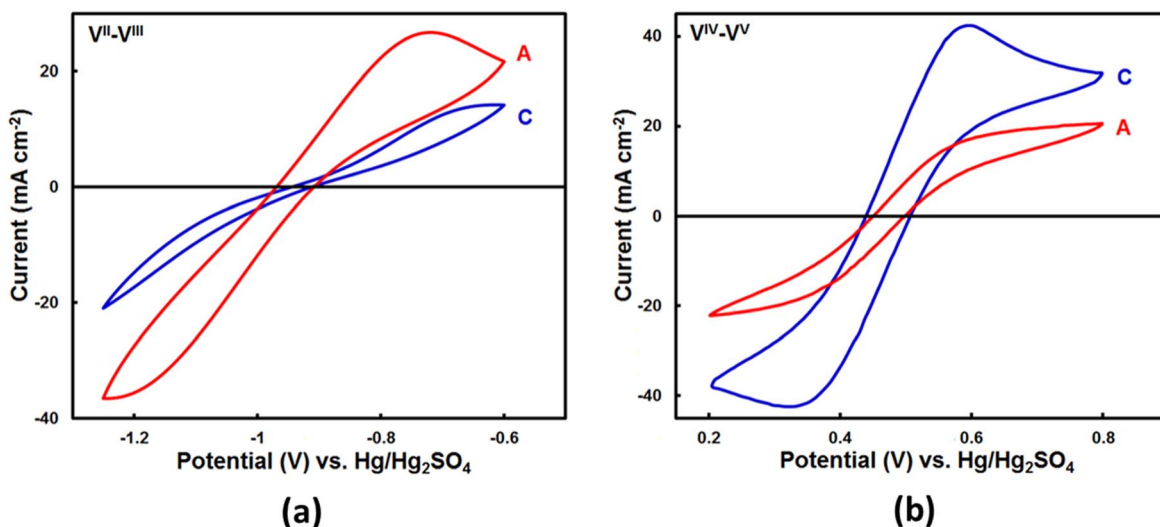


**Figure 1.** Comparison of CVs of a glassy-carbon electrode after anodic and cathodic treatments in (a) a  $V^{II}/V^{III}$  electrolyte and (b) a  $V^{IV}/V^V$  electrolyte. Curve A shows the steady-state CV after anodic treatment at +1.5 V for 60 s. Curve C shows the steady-state CV after cathodic treatment at  $-2.0$  V (in (a)) or  $-0.9$  V (in (b)) for 60 s. The scan rate was  $50 \text{ mV s}^{-1}$ . Further details in Refs. 15–17.

than its counterpart  $k_0^{23}$  for  $V^{II}/V^{III}$ . They noted however, that the observed reversibility of the  $V^{II}/V^{III}$  couple was critically linked to the surface pre-treatment of the glassy carbon electrode. No peaks could be observed in the cyclic voltametric response after polishing with P1200 SiC sandpaper, followed by 0.3 micron alumina and ultrasonic cleaning. When roughly polished with SiC paper however, distinct oxidation-reduction peaks could be observed highlighting the effect of surface roughness.<sup>93</sup> Many other studies qualitatively support the conclusion that the kinetics of  $V^{IV}/V^V$  are faster than those of  $V^{II}/V^{III}$ , although the reported ratios, as well as the values of the rate constants themselves (or equivalent measures such as exchange currents), often differ significantly. Studies have included CV measurements on a variety of different carbon substrates including glassy carbon, graphite, carbon papers and felts, carbon fibers, pyrolytic graphite, plastic formed carbon and others. Similar results have been reported for other techniques including linear sweep voltammograms (LSV) and EIS. However, there have also been a smaller number of reports that the kinetics of  $V^{IV}/V^V$  are slower than those of  $V^{II}/V^{III}$ .

Again, similar to results discussed in the previous section for flow cell experiments, large differences in the ratio of  $V^{II}/V^{III}$  and  $V^{IV}/V^V$  kinetic rates are often observed for the same electrode material after different pretreatments. For example Dixon et al.<sup>131</sup> reported that oxygen-plasma and thermal pretreatments of the electrode surfaces changed the kinetics of the vanadium reactions with significant improvements for  $V^{II}/V^{III}$ . Li et al.<sup>132</sup> reported that, following thermal pretreatment, LSVs were unchanged for  $V^{IV}/V^V$  but showed increased currents for  $V^{II}/V^{III}$ . Gattrell et al.<sup>98</sup> reported that polarisation curves for  $V^{IV}/V^V$  showed lower currents following electrochemical oxidising pretreatment of the electrode. Schmidt et al.<sup>133,134</sup> showed that, following electrochemical pretreatment, the charge transfer resistance of both couples decreased, with a more significant decrease observed for  $V^{II}/V^{III}$ ; the pretreatment consisted of 300 s at 2.2 V (RHE) (ca. 1.56 V (MSE)) for 300 s followed by 30 s at 0.1 V (RHE) (ca.  $-0.54$  V (MSE)).

**Effect of electrode treatment on the kinetics of  $V^{II}/V^{III}$  and  $V^{IV}/V^V$ .**—We have investigated<sup>15–18,89–91,120–122,135–138</sup> the effects of both anodic and cathodic treatment of carbon electrodes on the subsequent electrode kinetics of both  $V^{II}/V^{III}$  and  $V^{IV}/V^V$  using cyclic voltammetry (CV) and electrochemical impedance spectroscopy (EIS).

**Contrasting effects on  $V^{II}/V^{III}$  and  $V^{IV}/V^V$ .**—Typical results for  $V^{II}/V^{III}$  are shown in Fig. 1a; both CVs were obtained on the same

glassy-carbon electrode under the same conditions but after two different treatments. Curve A was obtained after the electrode had been anodically treated at +1.5 V for 60 s while Curve C was obtained after it had subsequently been cathodically treated at  $-2.0$  V for 60 s. (Unless otherwise stated, potentials are referenced to a saturated mercury-mercurous sulphate,  $\text{Hg}/\text{Hg}_2\text{SO}_4$ , electrode.) Clearly, the currents are much smaller in C than in A, indicating that the kinetics of  $V^{II}/V^{III}$  are inhibited by cathodic treatment. Subsequent anodic treatment at +1.5 V for 60 s again gave a CV similar to A. The behavior of the electrode could be “toggled” repeatedly in this way between a reduced state and an oxidized state with corresponding CVs similar to C and A, respectively.

Corresponding results for  $V^{IV}/V^V$  are shown in Fig. 1b. Again, Curve A was obtained after the electrode had been anodically treated at +1.5 V for 60 s while Curve C was obtained after it had been cathodically treated at  $-0.9$  V for 60 s. However, in sharp contrast with Fig. 1a, the currents are much larger in C than in A indicating that the kinetics of  $V^{IV}/V^V$  are enhanced by cathodic treatment.

Figure 2 shows results of experiments similar to those in Fig. 1 except that in this case EIS was used to monitor and quantify the electrode kinetics. Results for  $V^{II}/V^{III}$  are shown in Fig. 2a. Clearly, the charge transfer resistance is much larger in C (after cathodic treatment) than in A (after anodic treatment) confirming the results in Fig. 1a that the kinetics of  $V^{II}/V^{III}$  are inhibited by cathodic treatment. Corresponding results for  $V^{IV}/V^V$  are shown in Fig. 2b. In this case, the charge transfer resistance is much smaller in C (after cathodic treatment) than in A (after anodic treatment) confirming the results in Fig. 1b that the kinetics of  $V^{IV}/V^V$  are enhanced by cathodic treatment.

The reproducibility of these effects was excellent. Both CV and EIS experiments showed that alternate cathodization and anodization of the electrode repeatedly toggled its behavior as described, with cathodization always leading to inhibition of  $V^{II}/V^{III}$  and enhancement of  $V^{IV}/V^V$ . Thus, the results obtained in  $V^{II}/V^{III}$  electrolyte (Figs. 1a and 2a) are in direct contrast to those obtained in  $V^{IV}/V^V$  electrolyte (Figs. 1b and 2b): the rates of the  $V^{II}/V^{III}$  reactions were inhibited by cathodic treatment, while the rates of the  $V^{IV}/V^V$  reactions were enhanced by cathodic treatment.

**Effect of treatment potential.**—Similar effects to those illustrated in Figs. 1 and 2 were observed when the electrode was anodically or cathodically treated at other potentials. Nyquist plots for  $V^{IV}/V^V$  in Fig. 3a show the effects of (successively more negative) pretreatment potentials on an oxidized electrode and in Fig. 3b show the

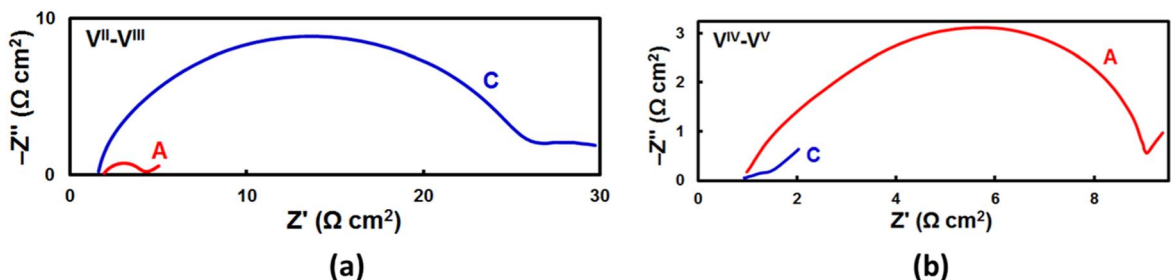


**Figure 2.** Comparison of Nyquist plots for a glassy-carbon electrode after anodic and cathodic treatments in (a) a  $V^{II}/V^{III}$  electrolyte and (b) a  $V^{IV}/V^V$  electrolyte. Curve A was obtained after anodic treatment at +1.5 V for 60 s. Curve C was obtained after cathodic treatment at (a) -2.0 V and (b) -0.9 V for 60 s. EIS were run at the rest potential with an a.c. amplitude of 10 mV. Further details in Refs. 15–17.

effects of (successively more positive) pretreatment potentials on a reduced electrode. Corresponding results for  $V^{II}/V^{III}$  for an oxidized and a reduced electrode are shown in Figs. 3c and 3d, respectively.

Normalized rate constants from experiments such as those in Fig. 3 are plotted against pretreatment potential in Fig. 4. The effect of cathodic pretreatment on the activity of a previously oxidized electrode is shown by curve  $C_{45}$  for  $V^{IV}/V^V$  and  $C_{23}$  for  $V^{II}/V^{III}$ , obtained from data such as Figs. 3a and 3c, respectively. Likewise, the effect of anodic pretreatment on a previously reduced electrode is shown by curve  $A_{45}$  for  $V^{IV}/V^V$  and  $A_{23}$  for  $V^{II}/V^{III}$ , obtained from data such as Figs. 3b and 3d, respectively.

The relationship between the normalized rate constant  $k'$  and the treatment potential  $E$  in each of the curves  $C_{45}$ ,  $C_{23}$ ,  $A_{45}$  and  $A_{23}$  can be approximately represented by an error-function-based equation of the form

$$k' = k'_{\min} + \frac{1 - k'_{\min}}{2} \left\{ 1 + \operatorname{erf} \left( \frac{E - E_m}{\sigma\sqrt{2}} \right) \right\} \quad [1]$$

with three adjustable parameters,  $k'_{\min}$ ,  $E_m$  and  $\sigma$ . The parameter  $k'_{\min}$  represents the value of the normalized rate constant  $k'$  at which the function levels off to a minimum;  $E_m$  represents the value of  $E$  at the midpoint value of  $k' = \frac{1}{2}(1 - k'_{\min})$ ; and  $\sigma$  is a standard deviation which controls the distribution of  $E$  about  $E_m$ . The lines in Fig. 4 show fits of Eq. 1 to the experimental data for glassy carbon. It can be seen that in all cases the curves represent a reasonable approximation to the data and in some cases, the fit is very good.

The curves  $C_{23}$  and  $A_{23}$  represent the potentials for the formation and decay of the reduced state R of the electrode. Clearly there is considerable hysteresis between these curves. This hysteresis reflects the slow kinetics of the formation and decay processes, and the equilibrium potentials must be intermediate between  $C_{23}$  and  $A_{23}$ . Assuming that the kinetics of formation and decay are similar, we can represent the equilibrium potentials as being midway between  $C_{23}$  and  $A_{23}$ . Such a midway curve can be constructed from Eq. 1 using the average values of the parameters  $k'_{\min}$ ,  $V_m$  and  $\sigma$  for  $C_{23}$  and  $A_{23}$ ; this curve is shown as  $E_{23}$  in Fig. 4. Similarly  $A_{45}$  and  $C_{45}$  represent the potential for the formation and decay, respectively, of the oxidized state O and we can construct the midway curve for O from the average of the parameters for  $A_{45}$  and  $C_{45}$  (curve  $E_{45}$  in Fig. 4).

The results in Fig. 4 are for glassy carbon but similar results are observed on many different types of carbon.<sup>15,136,137</sup> Typical results for carbon fiber, glassy carbon, carbon paper, and carbon xerogel are compared in Fig. 5. For clarity of presentation, the experimental data points are not shown. The curves were fitted to the data using Eq. 1 as before; the values of the fitting parameters  $k'_{\min}$ ,  $V_m$  and  $\sigma$  are shown in Table II. Thus, the results are quite general for many types of carbon and, regardless of the underlying mechanism, the conclusions are most important in the context of the VFBS.<sup>60</sup>

**Three states of carbon surfaces.**—Each of the four solid curves in Fig. 4 for glassy carbon (or, equivalently, the four broken curves in

Fig. 5 for the average of four carbons) represents a transition in electrode properties. Thus,  $C_{23}$  represents a transition to a reduced state (R) which has lower activity (lower  $k'$ ) for  $V^{II}/V^{III}$  oxidation/

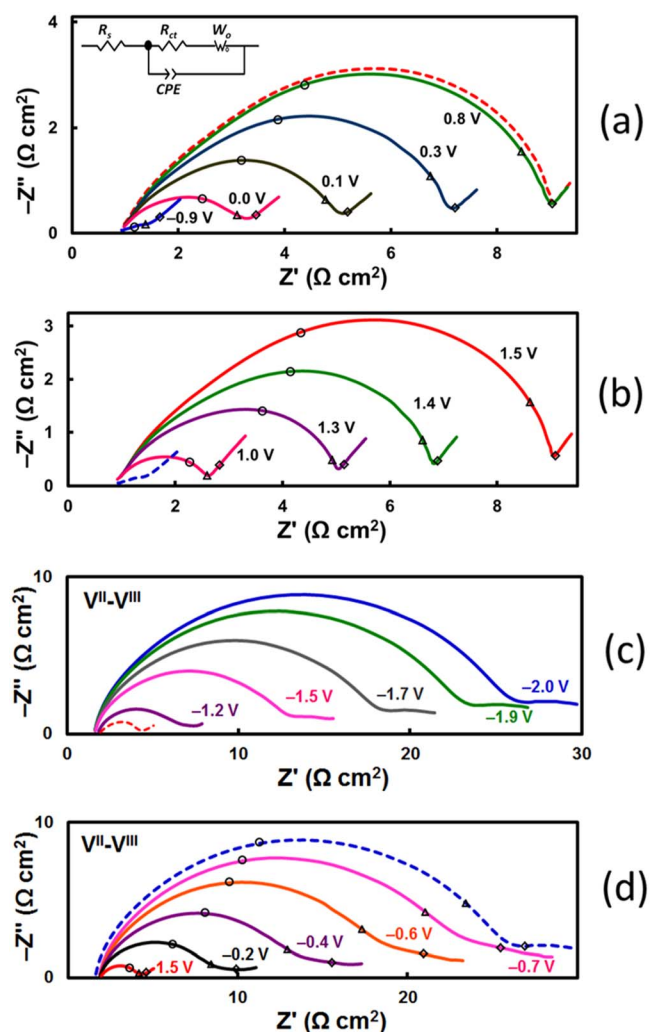


**Figure 3.** Nyquist plots for a glassy carbon electrode, after pretreatment at the potentials indicated: (a) and (b) in  $V^{IV}/V^V$ ; (c) and (d) in  $V^{II}/V^{III}$ . In (a) and (c), the pretreatment was cathodic and, prior to pretreatment at each of the potentials shown, the electrode was held for 60 s at a more positive potential (+1.5 V). In (b) and (d), the pretreatment was anodic and, prior to pretreatment at each of the potentials shown, the electrode was held for 60 s at a more negative potential (-0.9 V for (b) and -2.0 V for (d)). The electrolyte was 1:1  $V^{IV}/V^V$  or  $V^{II}/V^{III}$  in  $H_2SO_4$  with a total vanadium concentration of  $1.5 \text{ mol dm}^{-3}$  and a total sulphate concentration of  $4.5 \text{ mol dm}^{-3}$ . Potentials are referenced to a saturated  $Hg/Hg_2SO_4$  electrode (MSE). Further details in Refs. 15–17.

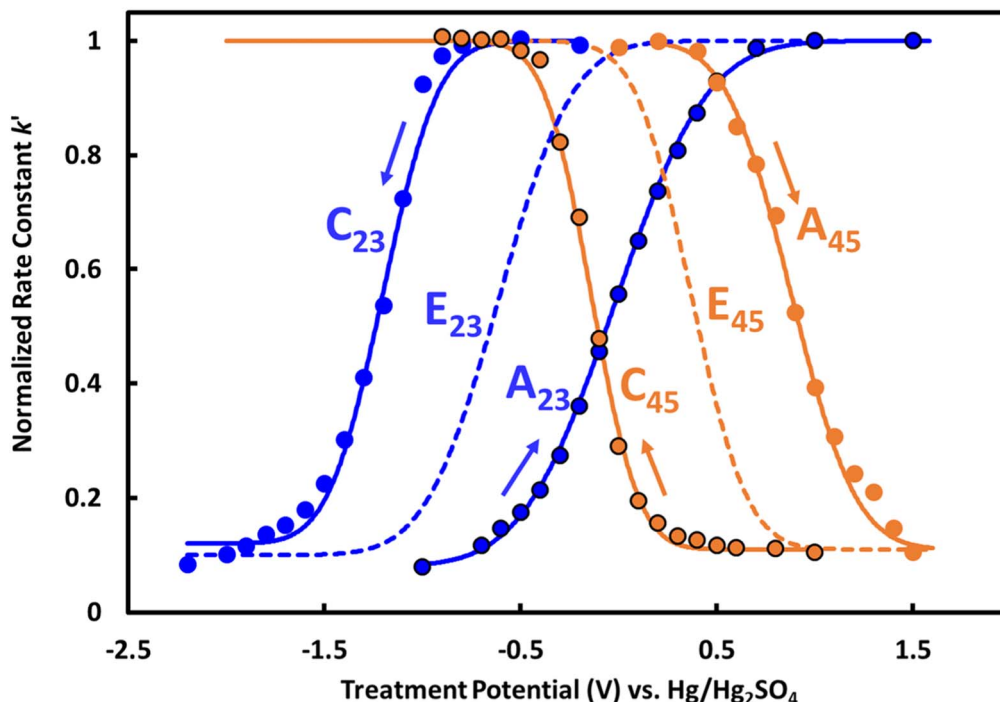


**Figure 4.** Normalised rate constant  $k' = k_c/k_{o,max}$  from EIS measurements on carbon fiber electrodes plotted against treatment potential. The data points on curves  $C_{45}$ ,  $A_{45}$ ,  $C_{23}$  and  $A_{23}$  correspond to measurements such as (a)–(d), respectively, in Fig. 3 and the lines represent fits of Eq. 1 to the data. The designations C and A represent cathodic and anodic treatments, respectively; blue lines represent  $V^{II}/V^{III}$  and orange lines represent  $V^{IV}/V^V$ ; down arrows represent deactivation and up arrows represent activation. Curves  $E_{23}$  and  $E_{45}$  represent the midway potentials for  $V^{II}/V^{III}$  and  $V^{IV}/V^V$ , respectively, as described in the text. Further details in Refs. 15–17.

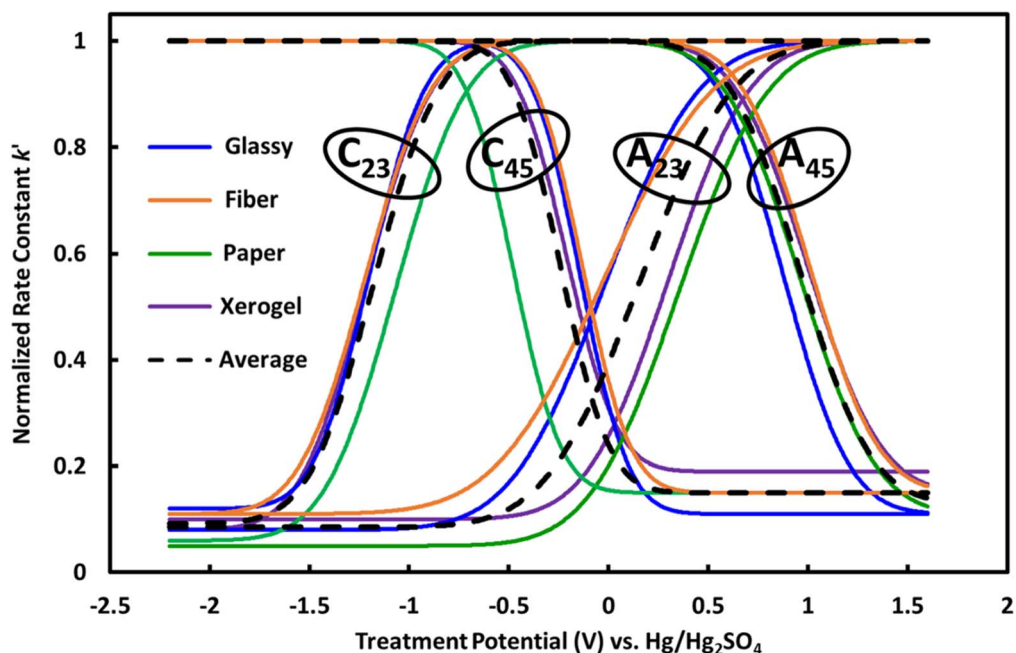


**Figure 5.** Plots, as in Fig. 4, for four types of carbon as indicated; the curve fitting parameters are shown in Table II. The broken lines represent averages for the four carbons, calculated using Eq. 1 and Table II. Further details in Refs. 15–17.

reduction and  $A_{45}$  represents a transition to an oxidized state (O) which has lower activity for  $V^{IV}/V^V$ . Likewise,  $C_{45}$  represents a transition to a reduced state (R') which has higher activity for  $V^{IV}/V^V$  and the  $A_{23}$  represents a transition to an oxidized state (O') which has higher activity for  $V^{II}/V^{III}$ .

The state O is formed at potentials  $\sim 1.2$  V more positive than those for O' and therefore O must be a more oxidized state than O'.

Likewise R must be a more reduced state than R'. In terms of potential  $O > O'$  and  $R < R'$ . In the absence of any evidence of a transition from O' to R' it seems reasonable to assume that O' and R' are the same state, call it meso (M); i.e.  $O' = R' = M$ . If this is so, then there are just three types of states of the electrode,  $R < M < O$  in order of increasing oxidation. The active state for both couples,  $V^{II}/V^{III}$  and  $V^{IV}/V^V$ , is the same state, M.

**Table II. Fitting parameters  $k'$ ,  $E_m$  and  $\sigma$  for the data in Fig. 5.**

		Glassy	Paper	Fiber	Xerogel	Average
C <sub>23</sub>	$k'$	0.12	0.06	0.11	0.08	0.0925
	$E_m/V$	-1.2	-1.07	-1.22	-1.22	-1.1775
	$\sigma/V$	0.22	0.28	0.26	0.26	0.255
A <sub>23</sub>	$k'$	0.08	0.05	0.11	0.1	0.085
	$E_m/V$	-0.02	0.35	-0.02	0.3	0.1525
	$\sigma/V$	0.37	0.35	0.43	0.32	0.3675
C <sub>45</sub>	$k'$	0.11	0.15	0.15	0.19	0.15
	$E_m/V$	-0.14	-0.48	-0.13	-0.21	-0.24
	$\sigma/V$	-0.19	-0.19	-0.19	-0.2	-0.1925
A <sub>23</sub>	$k'$	0.11	0.11	0.15	0.15	0.13
	$E_m/V$	0.88	0.96	1.01	1	0.9625
	$\sigma/V$	-0.26	-0.3	-0.27	-0.29	-0.28

These three states, R, O and M, of the electrode are represented in Fig. 6. The green region on the left represents the reduced state R of the electrode. Since the potential for formation of R from M is represented by the curve C<sub>23</sub> (in Figs. 4 or 5) and the potential for decay of R to M is represented by the curve A<sub>23</sub>, we represent the potential of the notional boundary of R and M by the mid-point of the curve E<sub>23</sub> which represents the average of the potentials of C<sub>23</sub> and A<sub>23</sub>. Of course, the potential boundary is not sharp but is more properly represented by the curve E<sub>23</sub>. Additionally however, due to large hysteresis, potentials much more negative than E<sub>23</sub> are required to form R and potentials much more positive than E<sub>23</sub> are required to annihilate R. This is indicated by the green arrows in Fig. 6. We similarly represent the notional boundary of O and M by the mid-point of E<sub>45</sub> which represents the average of the potentials of C<sub>45</sub> and A<sub>45</sub>. Again, the boundary is not sharp and potentials much more positive and negative than E<sub>45</sub> are required for the formation and decay, respectively, of O as indicated by the orange arrows in Fig. 6.

The curves E<sub>23</sub> and E<sub>45</sub> in Fig. 6 are combined into a single curve in Fig. 7 to give a plot of electrocatalytic activity against potential. This shows that the carbon surface has its highest activity in the region of -0.03 V Hg/Hg<sub>2</sub>SO<sub>4</sub> (+0.61 V, SHE) and has lower electrocatalytic activity at both low and high potentials. The curve approximates the theoretical activity at equilibrium at any potential but because of slow kinetics, as discussed, electrodes may often be in a metastable state and be considerably more or less active than their equilibrium value at that potential. Nevertheless, the curve gives us a benchmark against which to compare the effect of potential on electrocatalytic activity. Figure 7 also shows the values<sup>60</sup> of standard potential  $E^0$  for the V<sup>II</sup>/V<sup>III</sup> and V<sup>IV</sup>/V<sup>V</sup> couples. It can be seen that V<sup>II</sup>/V<sup>III</sup> is at a potential where the nominal activity of carbon is low whereas V<sup>IV</sup>/V<sup>V</sup> is at a potential where it is much higher. Based on this, we would expect the negative electrode in a VRB to be more prone to kinetic limitations than the positive.

In this three-state model, R is a low-activity state for both the V<sup>II</sup>/V<sup>III</sup> and V<sup>IV</sup>/V<sup>V</sup> couples but it is difficult to observe in the V<sup>IV</sup>/V<sup>V</sup> electrolyte because, under the oxidizing conditions, it is rapidly converted to M in the time-scale of the experiments. Likewise, O is a low-activity state for both couples but it is difficult to observe in the V<sup>II</sup>/V<sup>III</sup> electrolyte because, under the reducing conditions, it is rapidly converted to M. Nevertheless, there is recent evidence<sup>121,138</sup> that R is a low-activity state for V<sup>IV</sup>/V<sup>V</sup> and that O is a low-activity state for V<sup>II</sup>/V<sup>III</sup>.

The three-state model is consistent with other studies in the literature. As early as 1955, Garten and Weiss,<sup>139</sup> building on even earlier work, characterized three separate states of carbon. These consist of an ‘‘H’’ state obtained by pretreatment in moist and then dry air at higher temperatures (~800 °C), an ‘‘L’’ state obtained at lower temperatures (~400 °C), and a ‘more usual structure [is] intermediate between the ‘‘L’’ and ‘‘H’’ extremes’. They showed that the ‘‘L’’ carbon had acidic surface groups (which they proposed to be phenolic in nature) and that electrochemical reduction of ‘‘H’’ carbon greatly increased the acidity of its surface (i.e., it developed ‘‘L’’ characteristics). More recently, several groups<sup>140–142</sup> have made detailed studies of the activation of glassy carbon electrodes by

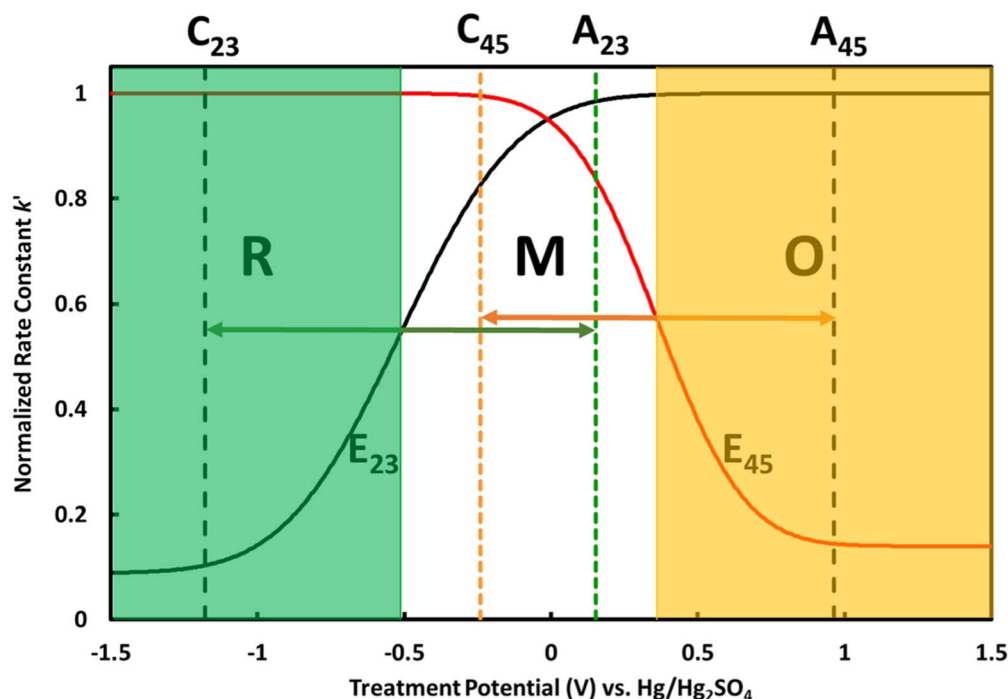


**Figure 6.** States of activity of a carbon electrode as a function of treatment potential. The reduced state R is shown in green, the oxidized state O in orange and the intermediate state M in white. The data represents an average of the four carbons studied. The line E<sub>23</sub> is the V<sup>II</sup>/V<sup>III</sup> midway curve (as described in the text) calculated from the average of C<sub>23</sub> and A<sub>23</sub> (broken lines in Fig. 5); similarly, E<sub>45</sub> represents the corresponding V<sup>IV</sup>/V<sup>V</sup> midway curve. The broken vertical lines represent the potentials at the mid-points of the curves C<sub>23</sub>, C<sub>45</sub>, A<sub>23</sub> and A<sub>45</sub> (broken lines in Fig. 5).

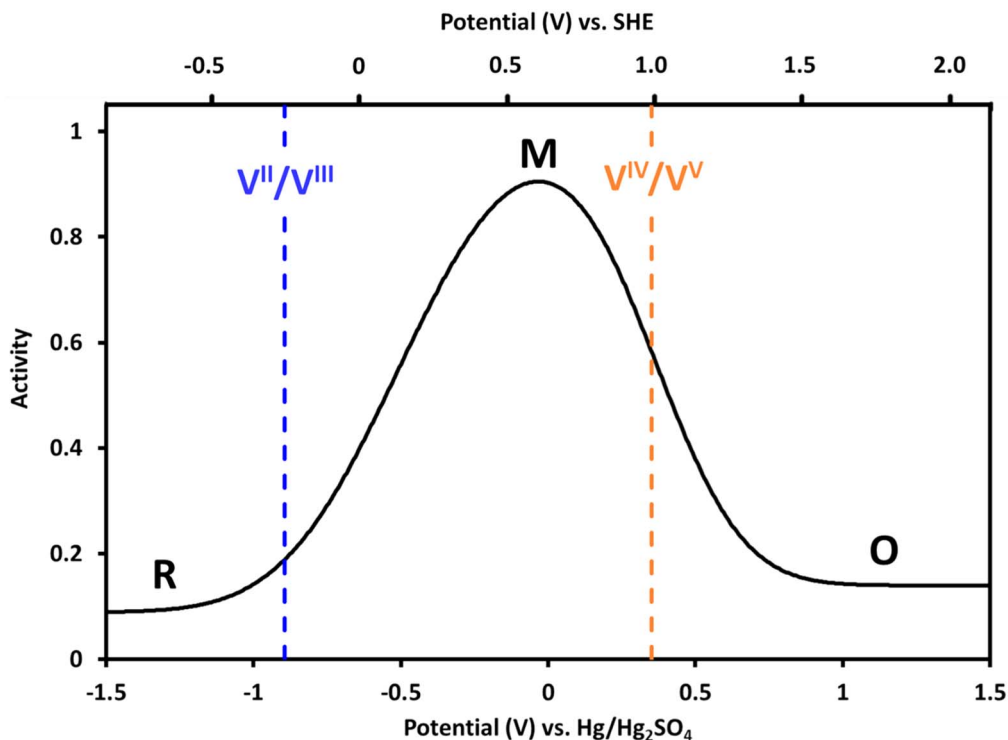


**Figure 7.** Electrochemical activity plotted against potential. The values of  $k'_{23}$  and  $k'_{45}$  in curves E<sub>23</sub> and E<sub>45</sub>, respectively, in Fig. 6 are multiplicatively combined into a single curve representing, in arbitrary units, activity  $a = k'_{23}k'_{45}$ . The standard electrode potentials<sup>60</sup>  $E^0 = -0.255$  and  $0.991$  V (SHE) for  $V^{II}/V^{III}$  (blue - - -) and  $V^{IV}/V^{V}$  (orange - - -), respectively, are shown.

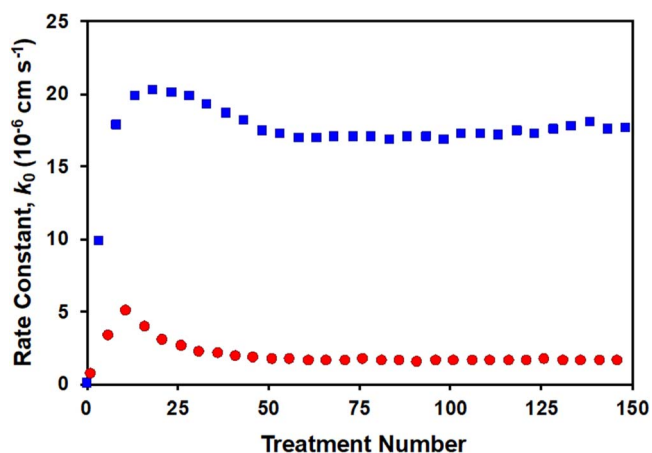


**Figure 8.** The electrochemical rate constant  $k_0$  for  $V^{IV}/V^{V}$  on a reduced (■) and oxidized (●) electrode plotted against the number of prior potential cycling treatments. Each treatment cycle consisted of 60 s at  $-0.9$  V (MSE) followed by 60 s at  $+1.5$  V (MSE). (From Ref. 143).

potential cycling. They used ellipsometry to show that a surface layer formed on the carbon surface and concluded that activation was due to a combination of effects including surface roughening, formation of a surface layer and reduction of this layer to form a porous hydrated structure.<sup>141</sup> They reported that reduction of the layer increased the activity but that extensive reduction led to deactivation of the surface.<sup>140</sup> This observation is also consistent with the R-M-O model.

*Effects of initial potential cycling.*—To establish surface conditions where these electrode states are quantitatively reproducible when toggling between them, repeated cycles of anodization/cathodization may be initially required. Typical behaviour<sup>137,138,143</sup> is illustrated in Fig. 8 where the activity of an as-received glassy

carbon electrode for  $V^{IV}/V^{V}$ , after anodic and cathodic pretreatments, respectively, is plotted as a function of its potential cycling history. Initially, the activity in each state increases markedly with cycling but quickly reaches a peak and levels off after about 40 cycles. Thus, repeated oxidation/reduction cycles irreversibly change the electrode surface until it eventually reaches a steady-state condition. In that condition, further application of the cycling pretreatment has little effect, but the electrode can now be toggled repeatedly and reproducibly between an activated (M) state and a deactivated (O) state by pretreatment at the appropriate potential. Similar behavior is observed for  $V^{II}/V^{III}$  and a steady state condition is reached where the electrode can be toggled between, in this case, an activated (M) state and a deactivated (R) state.

This pattern of behaviour of activity after reductive and oxidative pretreatment is qualitatively similar regardless of the previous history of the electrode. Quantitatively however, it strongly depends not only on the particular type of carbon but also on its history. Thus, both the absolute and relative magnitudes of activity towards the  $V^{II}/V^{III}$  and  $V^{IV}/V^{V}$  redox reactions depend on the irreversible effects of earlier potential cycling to which the electrode had been exposed as well as on the particular potentials at which the electrode was recently treated. For example, an electrode will always be activated for the  $V^{IV}/V^{V}$  reaction by appropriate reductive pretreatment; however the magnitude of the effect will strongly depend not only on the pretreatment potential at which it is reduced, but also on the potential regime to which it has been exposed before reduction. Likewise, an electrode will always be activated for the  $V^{II}/V^{III}$  reaction by appropriate oxidative pretreatment; however the magnitude of the effect will strongly depend not only on the pretreatment potential at which it is oxidized, but also on the potential regime to which it has been exposed before oxidation.

*Comparison of various studies of electrochemical pretreatments.*—The above observations of the contrasting effects of electrochemical pretreatments on the  $V^{II}/V^{III}$  and  $V^{IV}/V^{V}$  reactions are consistent with several other studies, mostly on glassy carbon

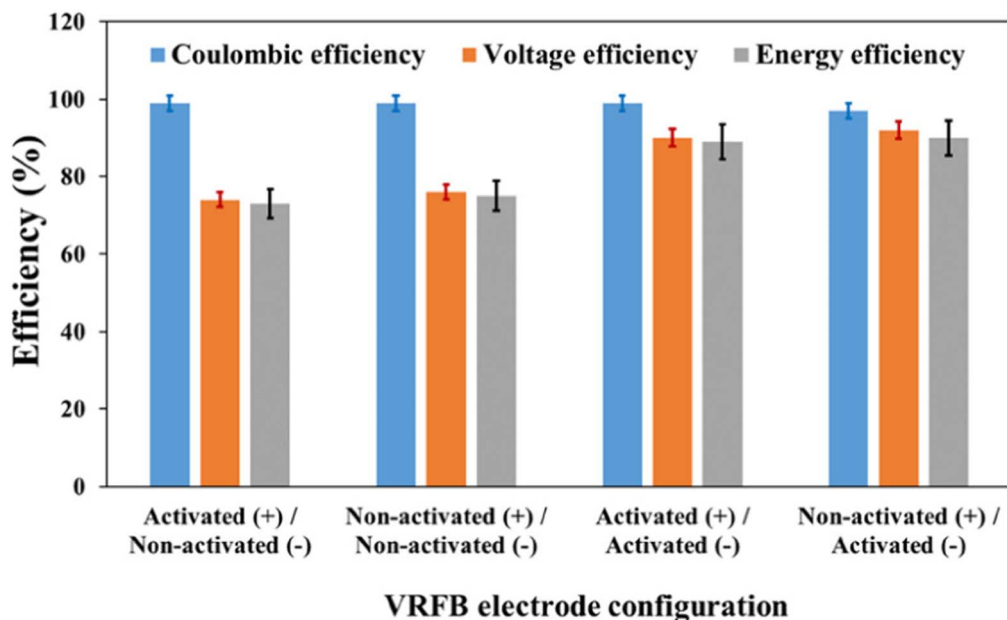


**Figure 9.** Energy efficiencies, coulombic efficiencies, and voltage efficiencies of VFBs with various electrode configurations. Reprinted with permission from Ref. 132. Copyright © 2019 American Chemical Society.

electrodes. In a detailed study of surface pretreatment, Skyllas-Kazacos and coworkers<sup>144</sup> demonstrated the effect of surface roughening and defect formation in enhancing the activity of glassy carbon electrodes towards the  $V^{IV}/V^V$  reaction. They reported that the enhancement of surface activity initially observed after anodic pretreatment was due to surface roughening and defect formation. They also confirmed that the concomitant surface oxidation inhibited, rather than enhanced, the activity of electrodes for the  $V^{IV}/V^V$  reaction and reported X-ray photoelectron spectroscopy (XPS) measurements that supported this conclusion. Their work also confirmed that cathodic pretreatment then enhances electrode activity for  $V^{IV}/V^V$ . Taylor et al.<sup>133</sup> drew similar conclusions supported by Raman as well as XPS measurements. In an early study, Gattrell et al.<sup>98</sup> also reported evidence that anodic pretreatment decreased the activity of glassy carbon and pyrolytic graphite electrodes for  $V^{IV}/V^V$ . Recently, Noack et al.<sup>145</sup> reported an extensive study of the effects electrochemical pretreatment of glassy carbon electrodes on subsequent  $V^{IV}/V^V$  and  $V^{II}/V^{III}$  kinetics, supported by confocal microscopy and XPS measurements.

As regards the  $V^{II}/V^{III}$  reaction, Taylor et al.<sup>134</sup> reported that anodic pretreatment enhanced the activity of glassy carbon electrodes for oxidation of  $V^{II}$  and correlated this with an increased presence of oxygen functional groups on the surface observed by XPS. They also reported that pretreating the electrode by cycling to, or holding at, negative potentials caused a loss of activity for  $V^{II}/V^{III}$ . In later work,<sup>146</sup> they investigated the activity and faradaic efficiency of oxidized edge and basal plane pyrolytic graphite electrodes. They concluded that oxygen functional groups play a catalytic role, improving reaction kinetics independent of the initial type of carbon used. In earlier work, McCreery and coworkers<sup>147</sup> also reported enhancement of the  $V^{II}/V^{III}$  reaction by electrochemical oxidation of glassy carbon electrodes.

**Thermal and chemical pretreatments of electrodes.**—These results are also consistent with reports of thermal pretreatments in air which are generally found to significantly enhance the  $V^{II}/V^{III}$  reaction while either inhibiting or having little effect on the  $V^{IV}/V^V$  reaction, often despite surface area increases. Thermal pretreatment of VFB electrodes was identified early as a method to improve electrode performance. In early work on the energy efficiency of a

VFB, Skyllas-Kazacos's group identified optimal pretreatment conditions of 400 °C for 30 h in air for graphite felt.<sup>110</sup> Many other groups have reported similar results. Most commonly, thermal pretreatments are in air or in an oxygen-containing atmosphere,<sup>112,123,148</sup> in some studies, the improvement in performance has been shown to increase with increasing concentration of oxygen in the gas mixture.<sup>38</sup> There is considerable recent evidence<sup>132</sup> that the primary effect of thermal activation of carbon is to reduce the overpotential at the negative electrode.

For example, Ramani's group<sup>132</sup> recently showed that the voltage and energy efficiency of a VFB increased significantly when the carbon used in the negative electrode had been thermally activated whereas no significant corresponding effect was observed for the positive (see Fig. 9). They reported that thermal activation of carbon felt electrodes at 400 °C in air for 30 h enhanced  $V^{II}/V^{III}$  kinetics while inhibiting  $V^{IV}/V^V$  kinetics. Similar results were also reported by Stimming and coworkers<sup>149</sup> using two different graphite felts; they also observed that the trends for the two redox reactions were always opposite: effects that increased the kinetics of  $V^{II}/V^{III}$  decreased the kinetics of  $V^{IV}/V^V$ . Several other authors<sup>123,125,131</sup> have similarly reported large improvements in  $V^{II}/V^{III}$  kinetics after thermal or plasma oxidation of felt electrodes with either a decrease or little change in  $V^{IV}/V^V$  kinetics despite surface area increases or structural changes. Likewise, Shao-Horn and coworkers<sup>127</sup> reported that heat-treatment of carbon paper at 400 °C for 30 h in air strongly enhanced  $V^{II}/V^{III}$  kinetics but did not have a notable influence on  $V^{IV}/V^V$  kinetics despite a large surface structural change. They further noted that scanning the potential of an untreated electrode to positive potentials also significantly enhanced the  $V^{II}/V^{III}$  kinetics but no such effect was observed on an electrode that had already been thermally oxidized.

Hydrothermal pretreatments of graphite felts in an ammonia<sup>150</sup> or urea<sup>151</sup> solution and high temperature pretreatment in ammonia gas<sup>152</sup> have also been reported to give improvements in VFB performance. The increased activity has been attributed to formation of nitrogen functional groups on the carbon surface. Likewise, chemical pretreatments<sup>106,110,153–155</sup> of electrodes have been reported to improve the efficiency of VFBs. For example, pretreatment with Fenton's reagent (aqueous  $H_2O_2$ /ferrous sulphate) at ambient temperature for 3 h was reported<sup>106</sup> to increase the energy efficiency

from 68% to 74% while pretreatment with a 3:1 mixture of H<sub>2</sub>SO<sub>4</sub> and HNO<sub>3</sub> at 80 °C for 8 h was also reported<sup>153</sup> to give a significant improvement.

**Reaction mechanisms, surface processes and surface functional groups.**—Despite many studies on the kinetics of the vanadium redox reactions on carbon electrodes, the mechanisms are still not well understood. The nature and density of oxygen-containing or other functional groups on the surface can depend strongly on electrode pretreatment. These functional groups are often associated with edge sites<sup>127,156</sup> on the graphitic sheets in the carbon structure and so the ratio of edge to basal plane sites on the surface can have a strong influence. Shao-Horn and coworkers<sup>127</sup> attributed enhancement of the kinetic rates for V<sup>II</sup>/V<sup>III</sup> and V<sup>IV</sup>/V<sup>V</sup> reactions to an increase in the concentration of edge-carbon sites and to oxygen functional groups associated with these sites, from investigation of graphite foil, HOPG and carbon paper electrodes. XPS measurements revealed an increase in both the oxygen content and the non-sp<sup>2</sup> content of carbon surfaces that had enhanced kinetic rates. Park et al.<sup>156</sup> also highlighted the role of edge sites and basal planes for vanadium kinetics.

The nature and surface density of the various functional groups has been extensively studied.<sup>100,123,131,133,134,142,149,157</sup> These may not only directly influence the rate of the electron transfer reactions but also strongly influence the hydrophilicity of the surface.<sup>56,110</sup> This, in turn, is a major factor in the degree of surface wetting<sup>56,110,123,149</sup> and so can strongly influence the electrochemically active surface area.<sup>123,157</sup> In addition to these considerations, there are also reports that strong anodic pretreatment of glassy carbon can produce surface films of multi-atomic-layer thickness, proposed to be either graphitic oxide<sup>140</sup> or highly porous glassy carbon with high oxygen and water content.<sup>141,142</sup> In a mini-review,<sup>158</sup> Radinger analysed selected literature on the electrochemical and physicochemical properties of treated electrodes and suggested that the importance of oxygen functional groups may be overemphasised while other properties are neglected. Bachman et al.<sup>159,160</sup> also suggests that the electrocatalytically active sites may not be the oxygen functional groups, but are much more likely to be carbene-like sites at zigzag edges.

Various studies have investigated the mechanism of the electron transfer<sup>27,161</sup> reactions themselves. V<sup>II</sup>/V<sup>III</sup> has generally been proposed to involve inner-sphere electron transfer,<sup>125,147,149,162–164</sup> although there is some disagreement in the literature.<sup>132</sup> The proposal is consistent with the apparent sensitivity of the reaction to various oxygen functional groups on carbon. However, there does not appear to be agreement on the detailed mechanism or on the nature of the bridging groups involved. In a study of glassy carbon, McCreery et al.<sup>147</sup> have proposed an inner-sphere mechanism catalysed by surface carbonyl groups (C=O); they reported that surfaces with a large proportion of hydroxyl (–OH) groups had the lowest kinetic rates. Derr et al.<sup>162</sup> have also proposed an inner-sphere mechanism catalysed by surface carbonyl groups but inhibited by surface carboxyl (COOH) and hydroxyl groups. However, while Agarwal et al.<sup>163</sup> have also proposed an inner-sphere mechanism, they have suggested that it occurs via bridging through adsorbed chloride (in HCl) and hydroxyl (in H<sub>2</sub>SO<sub>4</sub>) groups. Similarly, Choi et al.<sup>125</sup> concluded from molecular dynamics simulations that the hydration shells of the ions act as a barrier for electron transfer but that a hydroxyl group lowers the activation energy by breaking the hydration shell and anchoring the vanadium ions onto the electrode surface, enabling an inner-sphere mechanism. Jiang et al.<sup>164</sup> have proposed that the adsorption and desorption processes are more facile at graphite surfaces modified by carboxyl groups rather than carbonyl groups and Stimming et al.<sup>149</sup> have suggested that the V<sup>II</sup>/V<sup>III</sup> reaction may be an inner-sphere reaction catalysed by surface oxides.

The V<sup>IV</sup>/V<sup>V</sup> electron transfer reaction has sometimes been regarded as possibly being outer sphere, but there appears to be no general agreement. Choi et al.<sup>125</sup> have proposed that it occurs by an outer-sphere mechanism based on its relatively fast kinetics and its supposedly weak dependence on surface functionalisation (although,

as seen above, it can be strongly inhibited by anodic pretreatment of the surface). They concluded that, unlike V<sup>II</sup>/V<sup>III</sup> where the hydration shells of the ions act as a barrier for electron transfer, the less-organised nature of the V<sup>IV</sup> and V<sup>V</sup> hydration shells allows for direct contact of the ions with the electrode surface for electron transfer without the aid of a functional group. Derr et al.<sup>162</sup> have also suggested that V<sup>IV</sup>/V<sup>V</sup> may be outer-sphere. However, Jiang et al.<sup>164</sup> have proposed that both the V<sup>II</sup>/V<sup>III</sup> and V<sup>IV</sup>/V<sup>V</sup> reactions involve inner-sphere mechanisms. They infer that the adsorption and desorption processes for all four vanadium species are more facile at graphite surfaces modified by carboxyl groups rather than carbonyl groups. From evaluation of solvent reorganisation energies calculated using the Marcus-Hush kinetic model, Ramani and coworkers<sup>132</sup> have also concluded that the V<sup>IV</sup>/V<sup>V</sup> reaction is inner-sphere; from similar considerations they have concluded that the V<sup>II</sup>/V<sup>III</sup> reaction mechanism is outer-sphere.

However, in a recent mini-review,<sup>161</sup> of electrochemical kinetic data for vanadium electrode reactions, Roznyatovskaya et al. have pointed out that many of the studies of electron transfer kinetics have been carried out at dilute concentrations of vanadium and so their applicability to the more concentrated electrolytes in flow batteries may be limited.

**Degradation of electrode performance.**—Degradation of VFB performance with time is typically observed: both the charge and energy capacities decrease significantly with cycling. This is due to a combination of factors which include charge imbalance between the positive and negative electrolytes and electrode degradation.<sup>157,162,165</sup> Roth and co-workers have studied electrode degradation in detail<sup>157</sup> using charge-discharge cycling experiments in flow cells incorporating reference electrodes in combination with EIS measurements and supported by SEM and XPS. They observed a performance loss of ~40% over 50 cycles but attributed only 10%–12% to electrode degradation; they attributed the remainder to electrolyte imbalance and ohmic resistances. Electrochemical degradation of the carbon felts was reported to take place principally during the first 15–20 cycles, corresponding to 5–6 days in an 11-day experiment. The consequent loss of performance was attributed primarily to the negative electrode; there was no significant loss of performance at the positive. However, reversing the polarity of the VFB to recover lost performance met with little success overall.

Based on measurements at fiber electrodes (from carbon felts), Miller et al.<sup>17</sup> reported that the negative electrode in a VFB can become deactivated for the V<sup>II</sup>/V<sup>III</sup> reaction in the potential range which it experiences and that an electrode can become activated for the V<sup>II</sup>/V<sup>III</sup> reaction at the redox potential of the positive electrolyte (V<sup>IV</sup>/V<sup>V</sup>). This suggests that interchanging the positive and negative electrodes in a flow cell would reduce the overpotential at the negative electrode and so improve the performance. The prediction was supported by flow-cell experiments which showed that the overpotential at a carbon felt negative electrode increased after cycling but then decreased significantly when the positive and negative electrolytes were interchanged. Similarly, Shao-Horn and coworkers<sup>127</sup> found that the V<sup>II</sup>/V<sup>III</sup> kinetic rates of both heat-treated and as-received carbon paper electrodes were enhanced following treatment in a V<sup>IV</sup>/V<sup>V</sup> electrolyte. Thus, periodic electrolyte interchange (or equivalent alternatives, such as overdischarge) show promise of being a practical means of improving the voltage efficiency of VFBs.<sup>166–169</sup> Such strategies may also have the effect of removing impurities from electrode surfaces; for example, anodic removal of trace deposits of copper metal<sup>170</sup> from the negative would tend to decrease the rate of any hydrogen-evolution side reactions. Recently Greese et al.<sup>168,171</sup> have proposed that adsorbed V<sup>2+</sup> also may play an important role.

### Thermal Stability of Positive Electrolytes

**Solubility of vanadium species: thermodynamics and kinetics.**—The solubility of each of the vanadium species,<sup>172</sup> V<sup>II</sup>,

$V^{III}$ ,  $V^{IV}$  and  $V^V$ , is an important factor affecting the energy density of VFBs. The  $V^{II}$ ,  $V^{III}$  and  $V^{IV}$  species (i.e.,  $V^{2+}$ ,  $V^{3+}$  and  $VO^{2+}$ ) are generally quite soluble in strongly acidic  $H_2SO_4$  or  $H_2SO_4$ -HCl solutions; generally their solubility increases with temperature and decreases with increasing acid concentration.<sup>173</sup> The thermal stability of the positive electrolyte (posolyte) in the charged condition can be a limiting factor for the performance of VFBs. The predominant  $V^V$  species<sup>174</sup> present in strongly acidic solutions is the pervanadyl ion  $VO_2^+$ . At the pH of typical VFB positive electrolytes, the solubility of vanadium (V) oxide,  $V_2O_5$ , is  $\sim 0.1 \text{ mol dm}^{-3}$  or less<sup>175</sup> and so  $VO_2^+$  is expected to be thermodynamically unstable in solution with respect to precipitation as  $V_2O_5$ . Nevertheless, posolytes with high concentrations of  $V^V$  ( $>1.5 \text{ mol dm}^{-3}$ ) in sulphuric acid can persist for very long periods of time. Thus, all practical  $V^V$  electrolyte concentrations are metastable. Precipitation is controlled by kinetics and it has been shown<sup>137,176–181</sup> that the induction time for precipitation of  $V_2O_5$  decreases exponentially both with increasing temperature and with increasing  $V^V$  concentration and also increases exponentially with increasing sulphate concentration. The stability of these metastable solutions (VFB posolytes) decreases, as expected, as the concentration of  $V^V$  increases.<sup>176–182</sup> Stability improves with increasing concentration of sulphate<sup>176–181,183</sup> and in the presence of certain additives<sup>10,181,184,185</sup> such as phosphates and arsenates.

**Stability of  $V^V$  in acidic solution.**—There have been several studies<sup>14,82,176–179,181–192</sup> of the stability of  $V^V$  in the posolyte of VFBs and several mechanisms of precipitation have been proposed. The process is thought to begin with the formation of polymeric species, possibly after the initial formation of a neutral  $V^V$  species. The pervanadyl ion  $VO_2^+$  is generally regarded as the most common  $V^V$  species at low pH,<sup>174</sup> but it is well known that polynuclear species tend to form at high concentrations of vanadium.<sup>191</sup> For example, dimerization of pervanadyl ion in  $H_2SO_4$  and  $HClO_4$  solutions has been studied by UV-vis, Raman and nuclear magnetic resonance (NMR) spectroscopy.<sup>193</sup>

Density functional theory (DFT) simulations<sup>72</sup> suggest that the pervanadyl ion exists in typical posolytes primarily as a pentacoordinated species  $[VO_2(H_2O)_3]^+$  which is somewhat more stable than the hexacoordinated species  $[VO_2(H_2O)_4]^+$ . On the basis of NMR measurements and DFT calculations, it has been proposed<sup>72</sup> that deprotonation of  $[VO_2(H_2O)_3]^+$  gives a neutral species  $VO(OH)_3$  known to be a precursor in the formation of  $V_2O_5$  gels<sup>194,195</sup> and therefore a plausible intermediate in the mechanism of precipitation of  $V_2O_5$  from VFB positive electrolytes. We have reported<sup>176–181</sup> that precipitation occurs after an induction time that shows Arrhenius dependence on temperature, and have derived a value of 1.79 eV for the activation energy ( $E^\ddagger$ ) of the induction process. Based on DFT calculations Vijakumar and coworkers<sup>72,190</sup> estimated that an energy barrier of  $\sim 1.25$  eV needs to be overcome to convert  $[VO_2(H_2O)_3]^+$  to  $VO(OH)_3$ . This value of energy is lower by only  $\sim 30\%$  than the value of activation energy that we obtain from our Arrhenius data: the difference could be explained easily as the difference in energy between  $VO(OH)_3$  and the activated complex leading to its formation.

**Variation with temperature and composition.**—Using a standard methodology we carried out a series of experiments<sup>176–180</sup> in which we measured the induction time for precipitation over a range of temperatures for an extensive range of concentrations of  $V^V$  and sulphate. For each composition examined, a plot of the logarithm of induction time against inverse temperature was linear and the slope was similar in all cases. We have shown elsewhere<sup>177</sup> that such plots are effectively Arrhenius plots and can be used to derive values of the Arrhenius slope  $m$ , which quantifies the variation with temperature.

The effect of  $V^V$  concentration is illustrated in Fig. 10a where induction time for posolytes with a constant concentration of sulphate is plotted against concentration of  $V^V$ . The straight-line behavior on this log-linear plot shows that induction time decreases

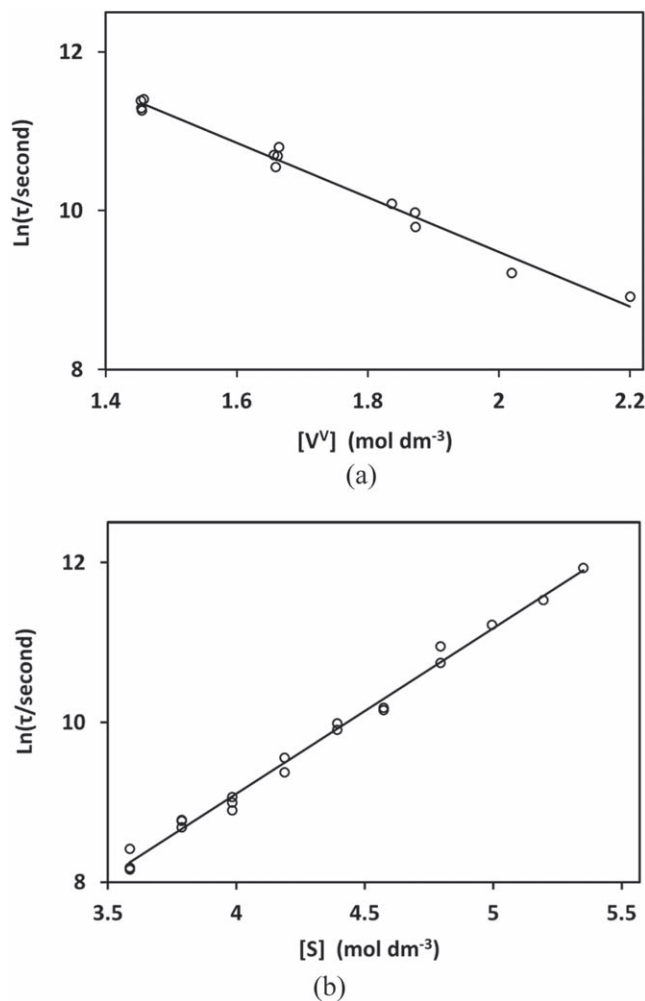


**Figure 10.** Natural logarithm of induction time at 50 °C plotted against (a)  $V^V$  concentration for a sulphate concentration of  $4.5 \text{ mol dm}^{-3}$ ; and (b) sulphate concentration for a  $V^V$  concentration of  $1.76 \text{ mol dm}^{-3}$ . (From Ref. 177).

exponentially with  $V^V$  concentration. A similar dependence on  $V^V$  concentration was observed for all sulphate concentrations examined. The slope  $\beta_{V^V}$  of the plot in Fig. 10a may be used to quantify the fractional rate of variation of induction time  $\tau$  with  $V^V$  concentration  $[V^V]$ :

$$\beta_{V^V} = \frac{\partial \ln \tau}{\partial [V^V]} = \frac{1}{\tau} \frac{\partial \tau}{\partial [V^V]} \quad [2]$$

We call  $\beta_{V^V}$  the  $V^V$  concentration coefficient of induction time.

The effect of sulphate concentration is illustrated in Fig. 10b where induction time for posolytes with a constant concentration of  $V^V$  is plotted against concentration of sulphate. The straight-line behavior on this log-linear plot shows that induction time increases exponentially with sulphate concentration. A similar dependence on sulphate concentration was observed for all  $V^V$  concentrations examined. The slope  $\beta_S$  of a log-linear plot such as that in Fig. 10b may be used to quantify the fractional rate of variation of induction time with sulphate concentration  $[S]$ :

$$\beta_S = \frac{\partial \ln \tau}{\partial [S]} = \frac{1}{\tau} \frac{\partial \tau}{\partial [S]} \quad [3]$$

We call  $\beta_S$  the sulphate concentration coefficient of induction time.

We can use the coefficients  $\beta_S$  and  $\beta_{V^V}$  to convert the measured induction time  $\tau$  at concentrations  $[S]$  and  $[V^V]$  to a standard value

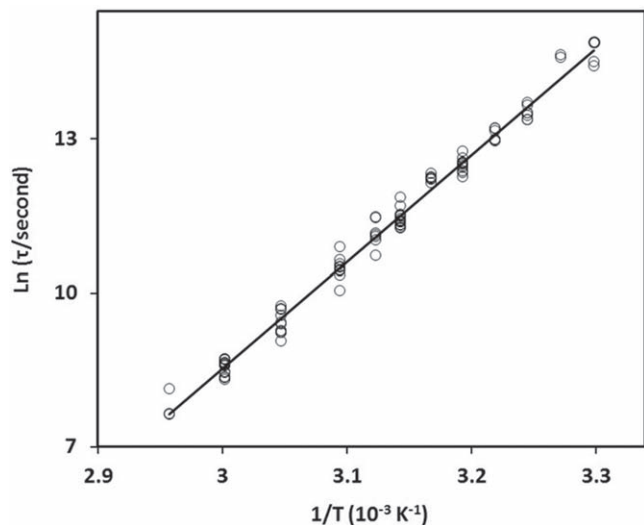


**Figure 11.** Arrhenius plot for 93 separate measurements of induction time for 23 different electrolyte solutions with  $V^V$  concentrations of  $1.4\text{--}2.2\text{ mol dm}^{-3}$  and sulphate concentrations of  $3.6\text{--}5.4\text{ mol dm}^{-3}$ . The measured induction times have been normalized to concentrations  $[S]_R = 4.5\text{ mol dm}^{-3}$  and  $[V^V]_R = 1.7\text{ mol dm}^{-3}$ . (From Ref. 177).

**Table III.** Concentrations of electrolyte used in Series A and Series B experiments. (From Ref. 196).

Species	Concentration ( $\text{mol dm}^{-3}$ )	
	Series A	Series B
Vanadium	1.601	1.600
Sulphate	4.147	4.165

$\tau_r$  with respect to reference concentrations  $[S]_r$  and  $[V^V]_r$  at the same temperature,  $T$ . Thus

$$\ln \tau_r = \ln \tau + \beta_S([S]_R - [S]) + \beta_{V5}([V^V]_R - [V^V]) \quad [4]$$

Using Eq. 4, 93 separate measurements of induction time for 23 different electrolyte solutions over a temperature range of  $30\text{--}65\text{ }^\circ\text{C}$  were standardized to reference concentrations  $[S]_R = 4.5\text{ mol dm}^{-3}$  and  $[V^V]_R = 1.7\text{ mol dm}^{-3}$ . An Arrhenius plot of the resulting values is shown in Fig. 11. The plot shows good linearity; the slope and intercept of the least-squares best-fit line are  $m = 20785\text{ K}$  and  $B_r = -53.828$  respectively. The standard error of estimate of the slope is  $238\text{ K}$  (1.1%); the activation energy estimated from the slope is  $E^\ddagger = (1.791 \pm 0.020)\text{ eV} = (172.8 \pm 1.9)\text{ kJ mol}^{-1}$ .

**Modelling electrolyte stability.**—The effects of temperature, vanadium concentration and sulphate concentration may be combined<sup>177</sup> in a single equation that expresses the induction time  $\tau$  for any posolyte as

$$\ln \tau = \ln \tau_{\text{std}} + m \left( \frac{1}{T} - \frac{1}{T_0} \right) + \beta_S([S] - [S]_R) + \beta_{V5}([V^V] - [V^V]_R) \quad [5]$$

with

$$\ln \tau_{\text{std}} = B_R + \frac{m}{T_0} \quad [5a]$$

where  $\tau_{\text{std}}$  is the value of  $\tau$  for the reference posolyte at a standard temperature  $T_0$  and  $B_R$  and  $m$  are, respectively, the intercept and

slope of its Arrhenius plot. Using Eq. 5, we can simulate the value of induction time for precipitation at a temperature  $T$  for any posolyte with concentrations of sulphate and  $V^V$  within the range of applicability of the equation. The results of such simulations agree well with the actual measured values: the root-mean-square (rms) deviation is 20% and the distribution of the deviation is about the same over the full range of induction times investigated ( $\sim 0.5\text{--}130$  hours).<sup>196</sup> However, the model is based on data measured for relatively short posolyte lifetimes. Thus, the measurements at lower temperatures were with less stable posolytes (i.e., high  $V^V$  concentration and low sulphate concentration) because the lifetimes of more stable posolytes were not measurable in the time-scale of the experiments.

We then extended our range of stability measurements to much longer times using an electrolyte composition close to that used in practical flow batteries. Two similar series of experiments, Series A and B, were carried out,<sup>196</sup> B being simply an independent repeat of A. Within each series, samples from the same posolyte were used in all experiments. The posolytes used in A and B had the same nominal concentrations although the precise values were slightly different (by 0.06% and 0.43%, respectively, for vanadium and sulphate): the measured concentrations are shown in Table III. In each series, the lifetime (i.e. the induction time for precipitation) was measured at 5-K increments over a temperature range of  $30\text{--}70\text{ }^\circ\text{C}$  with corresponding lifetimes ranging from 10.6 min to 86.7 days. The lifetimes were also simulated using the model based on our earlier (shorter-lifetime) data.<sup>177,180</sup>

The experimental results are compared with the simulations for both Series A and Series B in Fig. 12a. It can be seen that there is good agreement between the experimental results and the values predicted by the model at temperatures above  $\sim 45\text{ }^\circ\text{C}$ : the root-mean-square (RMS) average deviation is 20.6% for temperatures in the range of  $50\text{--}70\text{ }^\circ\text{C}$  compared with 60.6% in the range  $30\text{--}45\text{ }^\circ\text{C}$ . This is not surprising because the data on which the model is based were obtained for lifetimes of less than a week (higher temperatures and/or less stable electrolytes) whereas in Series A and B we have measured values of lifetime over a very wide range (10.6 min–86.7 days).

**Estimating the stable lifetime of electrolytes.**—It is clear from Fig. 12 that the Arrhenius slope is greater at lower temperatures (greater values of inverse temperature) than at higher temperatures. In Fig. 12b, the data is fitted with two least-squares best fit lines, one in the range  $30\text{--}45\text{ }^\circ\text{C}$  and another in the range  $50\text{--}70\text{ }^\circ\text{C}$ . The slopes of these lines are  $m_{lo} = 2.7850 \times 10^4\text{ K}$  ( $30\text{ }^\circ\text{C}\text{--}45\text{ }^\circ\text{C}$ ) and  $m_{hi} = 1.8967 \times 10^4\text{ K}$  ( $50\text{ }^\circ\text{C}\text{--}70\text{ }^\circ\text{C}$ ). The lines intersect at  $T_{\text{int}} = 45.5\text{ }^\circ\text{C}$  and  $\ln \tau_{\text{int}} = 10.8264$  ( $\tau = 5.0333 \times 10^4\text{ s}$ ). Thus, we can represent the lines in Fig. 12b by the equation

$$\ln \tau = \ln \tau_{\text{int}} + m \left( \frac{1}{T} - \frac{1}{T_{\text{int}}} \right) \quad [6]$$

where  $\tau$  is the lifetime at temperature  $T$ , and

$$m = \begin{cases} 2.2750 \times 10^4\text{ K} (T \leq T_{\text{int}}) \\ 1.8967 \times 10^4\text{ K} (T > T_{\text{int}}) \end{cases} \quad [6a]$$

The stable lifetimes of VFB posolytes are necessarily long (months or years in the charged condition) and so it is important to have a suitable means of sufficiently accelerating the aging process in such a way that the behaviour under the test conditions can be quantitatively related to behaviour under use conditions. Measurements at higher temperatures are an attractive method for accelerated testing of the stability of VFB posolytes. In order to extrapolate the results of such testing to use temperatures, estimates of the appropriate acceleration factors are needed. We can obtain such estimates using the above two-slope model. Values of acceleration factor  $f_T$  calculated using values of  $m_{hi} = 1.8967 \times 10^4\text{ K}$

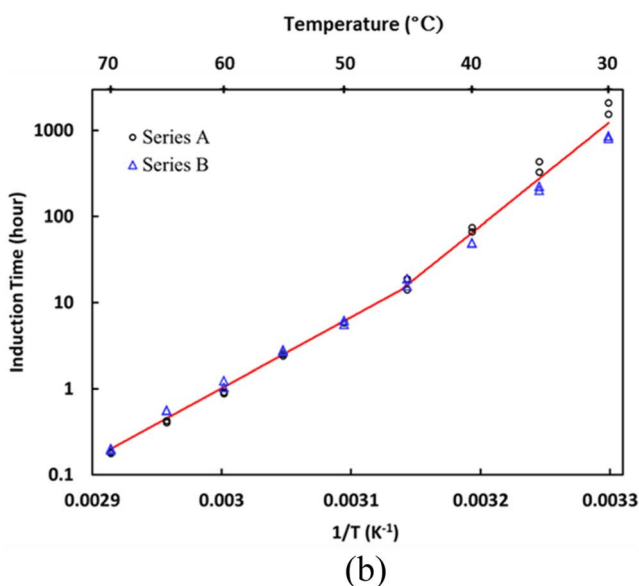
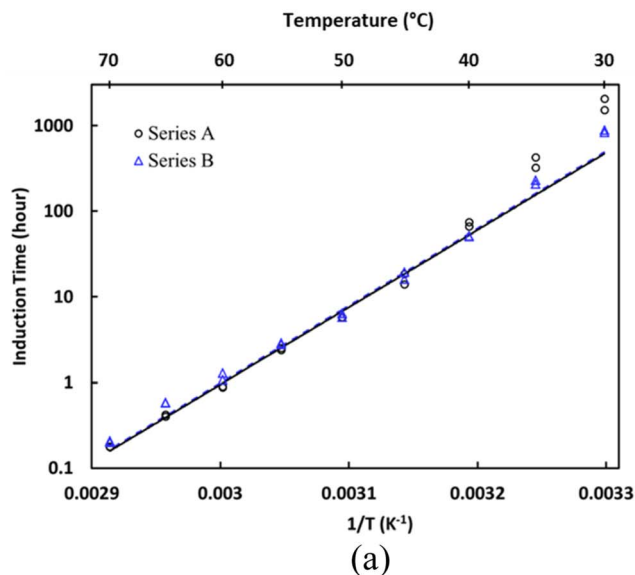


**Figure 12.** Arrhenius plots of experimental measurements for Series A and B: (a) comparison of measured induction times with simulations using our single-slope model which is based on other earlier results,<sup>177,180</sup> and (b) linear least-squares best-fit lines. Experimental results and simulations are represented, respectively, by the circles and the solid black line for Series A and by the triangles and the broken blue line for Series B. Best-fit lines are red. Lifetimes in (b) are adjusted to concentrations  $[V]_{\text{adj}} = 1.6 \text{ mol}^{-1} \text{ dm}^3$  and  $[S]_{\text{adj}} = 4.15 \text{ mol}^{-1} \text{ dm}^3$  using Eq. 4 since concentrations in Series A and B differed very slightly. (From Ref. 196).

and  $m_{10} = 2.7850 \times 10^4 \text{ K}$  are shown in Table IV for selected values of use temperature and test temperature.

**Effect of additives on the stability of the positive electrolyte.**—It has been reported<sup>14,184,185,197–199</sup> that certain additives can improve the thermal stability of VFB positive electrolytes. A great many additives have been suggested but evidence of their effectiveness is scarce. It is likely that most of these have little, if any, effect and/or are short-lived in the posolyte's acidic and oxidizing environment. We will briefly review two additives<sup>137,181,184,185</sup> which are effective for the stabilization of VFB posolytes: arsenate and phosphate.

The effect of added arsenate on the stability of  $V^V$  electrolytes was investigated using a standard accelerated testing methodology at temperatures in the range 30 °C–70 °C. At each temperature

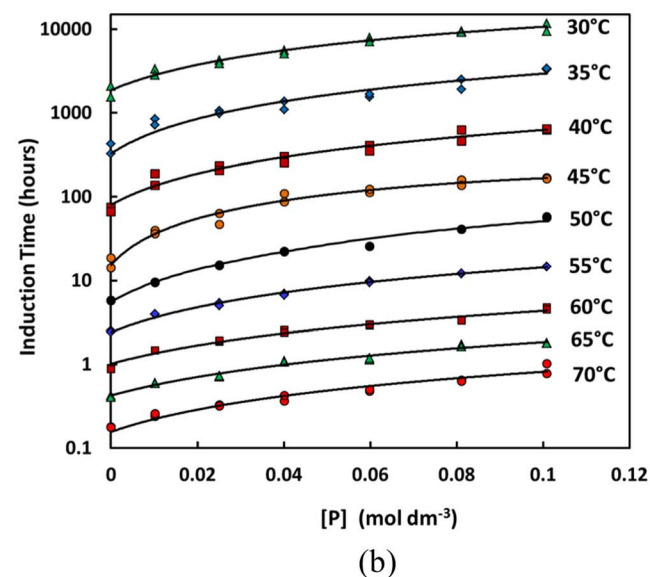
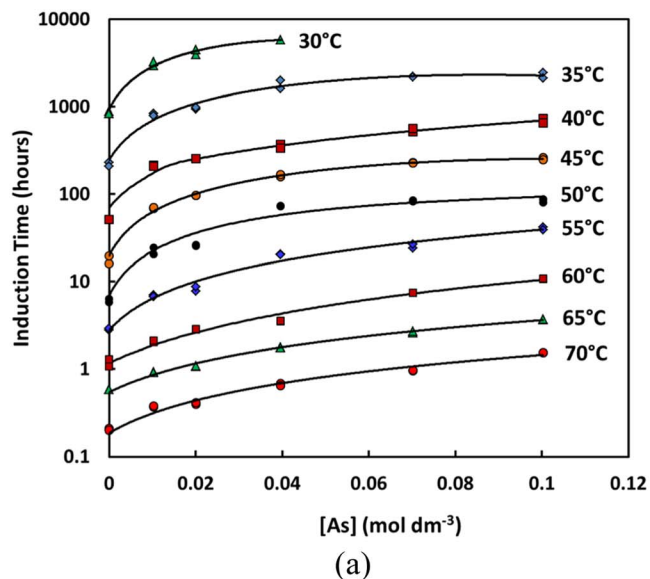


**Figure 13.** Induction time for precipitation of VFB posolyte plotted against the concentration of (a)  $\text{KH}_2\text{AsO}_4$  and (b)  $\text{H}_3\text{PO}_4$  for a series of temperatures. The posolyte solution was  $1.60 \text{ mol dm}^{-3} V^V$  in  $\text{H}_2\text{SO}_4$ ; the sulphate concentration was  $4.16 \text{ mol dm}^{-3}$ . (From Ref. 185).

investigated, the induction time for precipitation was measured for concentrations of arsenate ( $\text{KH}_2\text{AsO}_4$ ) from 0 (*i.e.* additive-free) to  $0.10 \text{ mol dm}^{-3}$ . The measured induction times are plotted against concentration of additive in Fig. 13a. A log-linear scale is used in order to show the values at each temperature on a single plot (values of induction time range from  $\sim 12$  min to 8 months). It can be seen that addition of the arsenate has a dramatic stabilizing effect on the electrolyte. For example, at 45 °C the additive-free electrolyte precipitates after 17.9 hours but the addition of  $0.040 \text{ mol dm}^{-3}$  arsenate increases this to 164 hours (a factor of 9.2) while the addition of  $0.10 \text{ mol dm}^{-3}$  increases it to 261 hours (a factor of 14.6). Likewise at 70 °C the additive-free electrolyte precipitates after  $\sim 12$  min but the addition of  $0.040$  and  $0.10 \text{ mol dm}^{-3}$  arsenate increases this time to 40 min and 1.54 hours (factors of 3.3 and 7.7), respectively.

The effect of added phosphate ( $\text{H}_3\text{PO}_4$ ) was similarly investigated. The results are shown in Fig. 12b. In agreement with previous reports,<sup>197,198</sup> it can be seen that the addition of phosphate has a strong stabilizing effect on the electrolyte. From

**Table IV.** Acceleration factors for use in estimating thermal stability at various use temperatures from data obtained at various test temperatures based on our two-slope model. The values are calculated based on slopes of  $m_{hi} = 1.8967 \times 10^4$  K and  $m_{lo} = 2.7850 \times 10^4$  K. (From Ref. 196).

Use temperature	Test temperature					
	50 °C	55 °C	60 °C	65 °C	70 °C	75 °C
	Acceleration factor ( $f_T$ )					
20 °C	4587	11220	26710	61980	140400	310400
25 °C	932.5	2280	5430	12600	28530	63100
30 °C	199.8	488.6	1163	2699	6112	13520
35 °C	45.00	110.0	262.0	608.0	1377	3045
40 °C	10.63	25.99	61.89	143.6	325.2	719.2
45 °C	2.627	6.425	15.30	35.50	80.38	177.8

Fig. 13b we see that the addition of 0.040 and 0.10 mol dm<sup>-3</sup> phosphate increases the induction time at 45 °C by factors of ~6 and ~10, respectively (compared with corresponding factors of 9.2 and 14.6 for arsenate). Likewise at 70 °C the induction time increases by factors of 2.2 and 5.1 with respect to the additive-free electrolyte for the addition 0.040 and 0.10 mol dm<sup>-3</sup> phosphate, respectively (compared with corresponding factors of 3.3 and 7.7 for arsenate). Thus, arsenate has a stronger stabilizing effect than phosphate. A combination of arsenate and phosphate is also effective.<sup>185</sup>

Although arsenate has a stronger stabilizing effect than phosphate, it is not likely to be a practical additive as it could deposit arsenic on the negative electrode. However, its effect is interesting because, like phosphate, it is a Group V element in a +5 oxidation state. Thus, observation of its effect may help us to understand the mechanism of electrolyte stabilization. In this regard, it is interesting to note that phosphorus is a known poison for vanadia-based catalysts.<sup>200</sup> While the mechanism of precipitation of V<sub>2</sub>O<sub>5</sub> from acidic V<sup>V</sup> solutions is not well understood, one may speculate that phosphorus (or arsenic) poisons the surface of embryonic crystals and so retards precipitation. We speculate that other Group-V elements (antimony and bismuth) may have similar effects. It may, however, be difficult to find compounds with antimony and bismuth in the +5 oxidation state which are stable and sufficiently soluble. We have tested nitrate (NO<sub>3</sub><sup>-</sup> added in the form of nitric acid) and found no stabilizing effect. This shows that the first-row Group-V element is different in this regard from its second- and third-row congeners.

## Conclusions

Electrodes for VFBs are typically fabricated from either carbon felt or carbon paper. The electrode kinetics of both the V<sup>II</sup>/V<sup>III</sup> and V<sup>IV</sup>/V<sup>V</sup> reactions on carbon have been examined in detail both in experimental flow cells and in conventional three-electrode cells. The kinetics are found to depend strongly on the pretreatment of the electrode. Typically, cycling an electrode between positive and negative potentials increases its roughness and activates it for both the V<sup>II</sup>/V<sup>III</sup> and V<sup>IV</sup>/V<sup>V</sup> reactions. Eventually, a steady state is reached where no further activation due to roughening is observed. However, activities for the V<sup>II</sup>/V<sup>III</sup> and V<sup>IV</sup>/V<sup>V</sup> reactions are strongly affected by the potential at which the electrode is held immediately prior to measurement and this effect is opposite for the two couples.

For the V<sup>II</sup>/V<sup>III</sup> reaction, *anodic* pretreatment *activates* the electrode and *cathodic* pretreatment *deactivates* it. The effects are reversible, although there is considerable hysteresis between the potentials for activation and for deactivation. In contrast, for the V<sup>IV</sup>/V<sup>V</sup> reaction, *anodic* pretreatment *deactivates* the electrode and *cathodic* pretreatment *activates* it. Again, the effects are reversible, with considerable hysteresis between the potentials for activation and for deactivation. These quantitatively reproducible and reversible effects are observed for a diverse variety of carbons including, importantly, fibers from graphite felts.

It is likely that enhancement of both V<sup>II</sup>/V<sup>III</sup> and V<sup>IV</sup>/V<sup>V</sup> is due to the same (active) state of the electrode. Oxidation of this active state leads to inhibition of V<sup>IV</sup>/V<sup>V</sup> while reduction of the same active state leads to inhibition of V<sup>II</sup>/V<sup>III</sup>. Inhibition of V<sup>IV</sup>/V<sup>V</sup> is not easily observed after strong cathodization because the strongly reduced state cannot persist for long under the oxidizing conditions of the V<sup>IV</sup>/V<sup>V</sup> electrolyte; likewise inhibition of V<sup>II</sup>/V<sup>III</sup> is not easily observed after strong anodization because the strongly oxidized state cannot persist for long under the reducing conditions of the V<sup>II</sup>/V<sup>III</sup> electrolyte.

The sensitivity to pretreatment makes comparison of V<sup>II</sup>/V<sup>III</sup> and V<sup>IV</sup>/V<sup>V</sup> kinetics difficult; however, V<sup>IV</sup>/V<sup>V</sup> kinetics are generally faster than V<sup>II</sup>/V<sup>III</sup> kinetics. The mechanisms of electron transfer have been the subject of several studies but are still not well understood. Many, but not all, investigators have suggested that the V<sup>II</sup>/V<sup>III</sup> electron transfer reaction occurs by an inner sphere mechanism. Some investigators have suggested that V<sup>IV</sup>/V<sup>V</sup> electron transfer occurs by an outer sphere mechanism but others have suggested an inner sphere mechanism. The nature and surface density of various functional groups on the electrode have been extensively studied. These may not only directly influence the rate of the electron transfer reactions but also strongly influence the degree of surface wetting and consequently the electrochemically active surface area. However, although there is much discussion on the importance of oxygen functional groups, it has also been suggested that other surface properties may be more important.

Although not the main factor, electrode degradation effects contribute to decreased performance of VFBs over time. Electrode degradation principally manifests itself as increased overpotential and there is evidence that it occurs mainly at the negative electrode. Reversing the polarity of the VFB has been suggested as one strategy to recover lost performance but not all investigators have found this strategy effective.

The V<sup>II</sup>, V<sup>III</sup> and V<sup>IV</sup> species (i.e., V<sup>2+</sup>, V<sup>3+</sup> and VO<sup>2+</sup>) in VFB electrolytes are quite soluble: generally their solubility increases with temperature and decreases with increasing acid concentration. However, the predominant V<sup>V</sup> species, VO<sub>2</sub><sup>+</sup>, present in charged positive electrolytes is thermodynamically unstable with respect to precipitation as V<sub>2</sub>O<sub>5</sub>. Precipitation is controlled by kinetics and the induction time for precipitation decreases with increasing temperature, showing an Arrhenius-type dependence. It also decreases exponentially with increasing V<sup>V</sup> concentration and increases exponentially with increasing sulphate concentration. From Arrhenius plots, a value of 1.79 eV is obtained for the activation energy ( $E^{\ddagger}$ ) of the induction process, in agreement with DFT calculations based on a VO(OH)<sub>3</sub> intermediate.

Based on measurements on many different electrolyte compositions over a temperature range of 30 °C–65 °C, a quantitative model was developed to predict the thermal stability as a function of temperature and concentrations. When longer-time measurement on electrolytes with compositions close to values in commercial flow batteries were included, an improved stability model (two-slope model) was formulated. The model can be used to estimate

acceleration factors for testing of electrolyte stability over a range of test and use temperatures.

Both arsenate and phosphate are effective additives for improving the thermal stability of VFB posolytes. A combination of arsenate and phosphate is also effective. Based on these results, we speculate that other Group-V elements in the +5 oxidation state may also stabilize VFB posolytes.

### Acknowledgments

We gratefully acknowledge the continued support of Enterprise Ireland, in particular Commercialisation Fund Grant No. CF 2018 0864 co-funded by the European Regional Development Fund (ERDF) under Ireland's European Union Structural and Investment Funds Programme 2014–2020. We also acknowledge support from the U.S. National Science Foundation, Sustainable Energy Pathways Program (NSF-1230236) and the Irish Research Council (IRC) and Sustainable Energy Authority of Ireland (SEAI).

### ORCID

Robert F. Savinell  <https://orcid.org/0000-0001-9662-2901>

Robert P. Lynch  <https://orcid.org/0000-0003-3547-5711>

D. Noel Buckley  <https://orcid.org/0000-0002-3006-8837>

### References

- M. J. Leahy, D. Connolly, and D. N. Buckley, *Wind Energy Storage Technologies, in Wind Power Generation and Wind Turbine Design*, ed. W. Tong (WIT Press, Southampton) p. 661 (2010).
- P. Duffy, C. Fitzpatrick, T. Conway, and R. P. Lynch, *Energy Sources and Supply Grids—The Growing Need for Storage, in Energy Storage Options and Their Environmental Impact*, ed. R. E. Hester and R. M. Harrison (The Royal Society of Chemistry) p. 1 (2018).
- H. Shao, P. Narayanasamy, K. M. Razeeb, R. P. Lynch, and F. M. F. Rhen, *Electrical Storage, in Energy Storage Options and Their Environmental Impact*, ed. R. E. Hester and R. M. Harrison (The Royal Society of Chemistry) p. 150 (2018).
- L. Joerissen, J. Garche, C. Fabjan, and G. Tomazic, *J. Power Sources*, **127**, 98 (2004).
- R. M. Darling, K. G. Gallagher, J. A. Kowalski, S. Ha, and F. R. Brushett, *Energy Environ. Sci.*, **7**, 3459 (2014).
- Z. Yang, J. Zhang, M. C. W. Kintner-Meyer, X. Lu, D. Choi, J. P. Lemmon, and J. Liu, *Chem. Rev.*, **111**, 3577 (2011).
- R. E. Hester and R. M. Harrison, *Energy Storage Options and Their Environmental Impact* (Royal Society of Chemistry) p. 1 (2018).
- T. A. Faunce, J. Prest, D. Su, S. J. Hearne, and F. Iacopi, *MRS Energy Sustain.*, **5**, 32 (2018).
- C. Roth, J. Noack, and M. Skyllas-Kazacos (ed.), *Flow Batteries: From Fundamentals to Applications* (New York, Wiley) (2022).
- M. Skyllas-Kazacos, M. H. Chakrabarti, S. A. Hajimolana, F. S. Mjalli, and M. Saleem, *J. Electrochem. Soc.*, **158**, R55 (2011).
- A. Z. Weber, M. M. Mench, J. P. Meyers, P. N. Ross, J. T. Gostick, and Q. Liu, *J. Appl. Electrochem.*, **41**, 1137 (2011).
- C. P. de Leon, A. Frias-Ferrer, J. Gonzalez-Garcia, D. A. Szanto, and F. C. Walsh, *J. Power Sources*, **160**, 716 (2006).
- M. J. Watt-Smith, P. Ridley, R. G. A. Wills, A. A. Shah, and F. C. Walsh, *J. Chem. Technol. Biotechnol.*, **88**, 126 (2013).
- S. Roe, C. Menictas, and M. Skyllas-Kazacos, *J. Electrochem. Soc.*, **163**, A5023 (2016).
- A. Bourke, M. A. Miller, R. P. Lynch, X. Gao, J. Landon, J. S. Wainright, R. F. Savinell, and D. N. Buckley, *J. Electrochem. Soc.*, **163**, A5097 (2016).
- A. Bourke, M. A. Miller, R. P. Lynch, J. S. Wainright, R. F. Savinell, and D. N. Buckley, *J. Electrochem. Soc.*, **162**, A1547 (2015).
- M. A. Miller, A. Bourke, N. Quill, J. S. Wainright, R. P. Lynch, D. N. Buckley, and R. F. Savinell, *J. Electrochem. Soc.*, **163**, A2095 (2016).
- A. Bourke, R. P. Lynch, and D. N. Buckley, *ECS Trans.*, **53**, 59 (2013).
- Y. Ashraf Gandomi et al., *J. Electrochem. Soc.*, **165**, A970 (2018).
- X. Ke, J. M. Prah, J. I. D. Alexander, J. S. Wainright, T. A. Zawodzinski, and R. F. Savinell, *Chem. Soc. Rev.*, **47**, 8721 (2018).
- M. Park, J. Ryu, W. Wang, and J. Cho, *Nat. Rev. Mater.*, **2**, 16080 (2016).
- E. Sánchez-Díez et al., *J. Power Sources*, **481**, 228804 (2021).
- K. Lourenssen, J. Williams, F. Ahmaddpour, R. Clemmer, and S. Tasnim, *J. Energy Storage*, **25**, 100844 (2019).
- C. Choi, S. Kim, R. Kim, Y. Choi, S. Kim, H.-Y. Jung, J. H. Yang, and H.-T. Kim, *Renew. Sustain. Energy Rev.*, **69**, 263 (2017).
- A. Cunha, J. Martins, N. Rodrigues, and F. P. Brito, *Int. J. Energy Res.*, **39**, 889 (2015).
- K. J. Kim, M.-S. Park, Y.-J. Kim, J. H. Kim, S. X. Dou, and M. Skyllas-Kazacos, *J. Mater. Chem. A*, **3**, 16913 (2015).
- T. V. Sawant, C. S. Yim, T. J. Henry, D. M. Miller, and J. R. McKone, *Joule*, **5**, 360 (2021).
- J. Noack, N. Roznyatovskaya, T. Herr, and P. Fischer, *Angew. Chem. Int. Ed.*, **54**, 9776 (2015).
- Q. Huang and Q. Wang, *ChemPlusChem*, **80**, 312 (2015).
- D. N. Buckley, C. O'Dwyer, N. Quill, and R. P. Lynch, *Electrochemical Energy Storage, in Energy Storage Options and Their Environmental Impact*, ed. R. E. Hester and R. M. Harrison (The Royal Society of Chemistry) p. 115 (2018).
- A. Z. Weber and T. Van Nguyen, *J. Electrochem. Soc.*, **163**, Y1 (2016).
- M. L. Perry and A. Z. Weber, *J. Electrochem. Soc.*, **163**, A5064 (2016).
- D. Reed, E. Thomsen, B. Li, W. Wang, Z. Nie, B. Koeppel, J. Kizewski, and V. Sprenkle, *J. Electrochem. Soc.*, **163**, A5211 (2016).
- H. H. Dewage, V. Yufit, and N. P. Brandon, *J. Electrochem. Soc.*, **163**, A5236 (2016).
- R. M. Darling, A. Z. Weber, M. C. Tucker, and M. L. Perry, *J. Electrochem. Soc.*, **163**, A5014 (2016).
- A. K. Manohar, K. M. Kim, E. Plichta, M. Hendrickson, S. Rawlings, and S. R. Narayanan, *J. Electrochem. Soc.*, **163**, A5118 (2016).
- C. R. Dennison, E. Agar, B. Akuzum, and E. C. Kumbur, *J. Electrochem. Soc.*, **163**, A5163 (2016).
- A. M. Pezeshki, R. L. Sacci, G. M. Veith, T. A. Zawodzinski, and M. M. Mench, *J. Electrochem. Soc.*, **163**, A5202 (2016).
- W. Duan et al., *J. Energy Chem.*, **27**, 1381 (2018).
- K. Yano, S. Hayashi, T. Kumamoto, T. Shibata, K. Yamanishi, and K. Fujikawa, *SEI Technical Review*, **84**, 22 (2017).
- A. Colthorpe, *Energy Storage News*, July 2022, <https://energy-storage.news/first-phase-of-800mwh-world-biggest-flow-battery-commissioned-in-china/>.
- H. Bindner, C. Ekman, O. Gehrke, and G. Tomazic, *Characterisation of Vanadium Flow Battery, Risk Report* (2011).
- G. Kear, A. A. Shah, and F. C. Walsh, *Int. J. Energy Res.*, **36**, 1105 (2012).
- K. L. Huang, X. G. Li, S. Q. Liu, N. Tan, and L. Q. Chen, *Renew Energy*, **33**, 186 (2008).
- M. Rychcik and M. Skyllas-Kazacos, *J. Power Sources*, **22**, 59 (1988).
- C. Fabjan, J. Garche, B. Harer, L. Jörissen, C. Kolbeck, F. Philipp, G. Tomazic, and F. Wagner, *Electrochim. Acta*, **47**, 825 (2001).
- A. Bhattarai, P. C. Ghimire, A. Whitehead, R. Schweiss, G. G. Scherer, N. Wai, and H. H. Hng, *Batteries*, **4**, 48 (2018).
- N. Poli, M. Schäffer, A. Trovò, J. Noack, M. Guarnieri, and P. Fischer, *Chem. Eng. J.*, **405**, 126583 (2021).
- C. Petchsingh, N. Quill, J. T. Joyce, D. Ní Eidhin, D. Oboroceanu, C. Lenihan, X. Gao, R. P. Lynch, and D. N. Buckley, *J. Electrochem. Soc.*, **163**, A5068 (2016).
- N. Quill, C. Petchsingh, R. P. Lynch, X. Gao, D. Oboroceanu, D. Ní Eidhin, M. O'Mahony, C. Lenihan, and D. N. Buckley, *ECS Trans.*, **64**, 23 (2015).
- D. N. Buckley, X. Gao, R. P. Lynch, N. Quill, and M. J. Leahy, *J. Electrochem. Soc.*, **161**, A524 (2014).
- D. N. Buckley, X. Gao, R. P. Lynch, M. J. Leahy, A. Bourke, and G. Flynn, *European Patent EP*, 13195315 (2013).
- X. Gao, R. P. Lynch, M. J. Leahy, and D. N. Buckley, *ECS Trans.*, **45**, 25 (2013).
- A. Parasuramana, T. M. Lima, C. Menictas, and M. Skyllas-Kazacos, *Electrochim. Acta*, **101**, 27 (2013).
- S. Zhong, C. Padeste, M. Kazacos, and M. Skyllas-Kazacos, *J. Power Sources*, **45**, 29 (1993).
- T. J. Rabbow, M. Trampert, P. Pokorny, P. Binder, and A. H. Whitehead, *Electrochim. Acta*, **173**, 17 (2015).
- T. J. Rabbow, M. Trampert, P. Pokorny, P. Binder, and A. H. Whitehead, *Electrochim. Acta*, **173**, 24 (2015).
- C. Minke, U. Kunz, and T. Turek, *J. Power Sources*, **342**, 116 (2017).
- D. S. Aaron et al., *J. Power Sources*, **206**, 450 (2012).
- D. N. Buckley, A. Bourke, N. Dalton, M. Alhaji Safi, D. Oboroceanu, V. Sasikumar, and R. P. Lynch, *Flow Batteries: From Fundamentals to Applications*, ed. C. Roth, J. Noack, and M. Skyllas-Kazacos (New York, Wiley) Chap. 24 (2022).
- N. Dalton, *Electrospun carbon nanofiber electrodes for vanadium flow batteries* (PhD Thesis, University of Limerick, Ireland) (2020).
- N. Dalton, R. P. Lynch, M. N. Collins, and M. Culebras, *Int. J. Biological Macromolecules*, **121**, 472 (2019).
- S. Liu, M. Kok, Y. Kim, J. L. Barton, F. R. Brushett, and J. Gostick, *J. Electrochem. Soc.*, **164**, A2038 (2017).
- A. Fetyan et al., *ChemElectrochem*, **2**, 2055 (2015).
- M. H. Chakrabarti et al., *J. Power Sources*, **253**, 150 (2014).
- D. Aaron, S. Yeom, K. D. Kihm, Y. A. Gandomi, T. Ertugrul, and M. M. Mench, *J. Power Sources*, **366**, 241 (2019).
- B. Li et al., *Nano Lett.*, **13**, 1330 (2013).
- T. Liu, X. Li, H. Zhang, and J. Chen, *J. Energy Chemistry*, **27**, 1292 (2018).
- M. Rychcik and M. Skyllas-Kazacos, *J. Power Sources*, **19**, 45 (1987).
- H. Kaneko, K. Nozaki, Y. Wada, T. Aoki, A. Negishi, and M. Kamimoto, *Electrochim. Acta*, **36**, 1191 (1991).
- M. Skyllas-Kazacos and F. Grossmith, *J. Electrochem. Soc.*, **134**, 2950 (1987).
- B. Fang, Y. Wei, T. Arai, S. Iwasa, and M. Kumagai, *J. Appl. Electrochem.*, **33**, 197 (2003).
- M. Vynnycky, *Energy*, **36**, 2242 (2011).
- N. Quill, D. Oboroceanu, J. O'Donnell, C. Lenihan, D. N. Buckley, and R. P. Lynch, *ECS Meet. Abstr.*, **MA2017-02**, 1 (2017).
- N. Quill, D. Oboroceanu, D. N. Buckley, and R. P. Lynch, *ECS Trans.*, **80**, 3 (2017).

76. M. Rybalchenko, N. Quill, D. N. Buckley, and R. P. Lynch, *ECS Trans.*, **109**, 131 (2022).
77. X. Gao, A. Bourke, R. P. Lynch, M. J. Leahy, and D. N. Buckley, *Conference Papers, The International Flow Battery Forum*, 20 (2013).
78. Z. Tang, D. S. Aaron, A. B. Papandrew, and T. A. Zawodzinski, *ECS Trans.*, **41**, 1 (2012).
79. M. Skyllas-Kazacos and M. Kazacos, *J. Power Sources*, **196**, 8822 (2011).
80. N. Quill, R. P. Lynch, X. Gao, and D. N. Buckley, *The Electrochemical Society Meeting Abstract*, **MA2014-01**, 389 (2014).
81. A. H. Whitehead and M. Harrer, *J. Power Sources*, **230**, 271 (2013).
82. F. Rahman and M. Skyllas-Kazacos, *J. Power Sources*, **189**, 1212 (2009).
83. M. Vijayakumar, W. Wang, Z. Nie, V. Sprengle, and J. Hu, *J. Power Sources*, **241**, 173 (2013).
84. D. N. Buckley et al., *ECS Trans.*, **109**, 3 (2022).
85. H. Prifti, A. Parasuraman, S. Winardi, T. M. Lim, and M. Skyllas-Kazacos, *Membranes*, **2**, 275 (2012).
86. C. Lenihan, D. Oboroceanu, N. Quill, D. Ní Eidhin, A. Bourke, R. P. Lynch, and D. N. Buckley, *ECS Trans.*, **85**, 175 (2018).
87. R. Darling, K. Gallagher, W. Xie, L. Su, and F. Brushett, *J. Electrochem. Soc.*, **163**, A5029 (2015).
88. Y. Shia, C. Eze, B. Xiong, W. He, H. Zhang, T. M. Lim, A. Ukilf, and J. Zhao, *Appl. Energy*, **238**, 202 (2019).
89. A. Bourke, R. P. Lynch, and D. N. Buckley, *ECS Trans.*, **64**, 1 (2015).
90. A. Bourke, N. Quill, R. P. Lynch, and D. N. Buckley, *ECS Trans.*, **61**, 15 (2014).
91. A. Bourke, N. Quill, R. P. Lynch, and D. N. Buckley, *Conference Papers, The International Flow Battery Forum*, **16** (2014).
92. G. Oriji, Y. Katayama, and T. Miura, *J. Power Sources*, **139**, 321 (2005).
93. E. Sum and M. Skyllas-Kazacos, *J. Power Sources*, **15**, 179 (1985).
94. E. Sum, M. Rychcik, and M. Skyllas-Kazacos, *J. Power Sources*, **16**, 85 (1985).
95. D. Aaron, C. N. Sun, M. Bright, A. B. Papandrew, M. M. Mench, and T. A. Zawodzinski, *ECS Electrochem. Letters*, **2**, A29 (2013).
96. C. N. Sun, F. M. Delnick, D. S. Aaron, A. B. Papandrew, M. M. Mench, and T. A. Zawodzinski, *ECS Electrochem. Letters*, **2**, A43 (2013).
97. J. W. Lee, J. K. Hong, and E. Kjeang, *Electrochim. Acta*, **83**, 430 (2012).
98. M. Gattrell, J. Park, B. MacDougall, J. Apte, S. McCarthy, and C. W. Wu, *J. Electrochem. Soc.*, **151**, A123 (2004).
99. A. Di Blasi, O. Di Blasi, N. Briguglio, A. S. Aricò, D. Sebastián, M. J. Lázaro, G. Monforte, and V. Antonucci, *J. Power Sources*, **227**, 15 (2013).
100. W. Li, J. Liu, and C. Yan, *Carbon*, **55**, 313 (2013).
101. W. Zhang, J. Xi, Z. Li, H. Zhou, L. Liu, Z. Wu, and X. Qiu, *Electrochim. Acta*, **89**, 429 (2013).
102. J. Xi, W. Zhang, Z. Li, H. Zhou, L. Liu, Z. Wu, and X. Qiu, *Int. J. Electrochem. Sci.*, **8**, 4700 (2013).
103. Y. Men and T. Sun, *Int. J. Electrochem. Sci.*, **7**, 3482 (2012).
104. X. G. Li, K. L. Huang, S. Q. Liu, N. Tan, and L. Q. Chen, *Transactions of Nonferrous Metals Society of China (English Edition)*, **17**, 195 (2007).
105. M. A. Miller, R. F. Savinell, and J. S. Wainright, *The Electrochemical Society Meeting Abstract*, **25**, MA2014-02 (2014).
106. L. Yue, W. Li, F. Sun, L. Zhao, and L. Xing, *Carbon*, **48**, 3079 (2010).
107. B. Sun and M. Skyllas-Kazacos, *Electrochim. Acta*, **37**, 2459 (1992).
108. E. Agar, C. R. Dennison, K. W. Knehr, and E. C. Kumbur, *J. Power Sources*, **225**, 89 (2013).
109. J. Friedl, C. Bauer, A. Rinaldi, and U. Stimming, *Carbon*, **63**, 228 (2013).
110. B. Sun and M. Skyllas-Kazacos, *Electrochim. Acta*, **37**, 1253 (1992).
111. Z. González, C. Botas, P. Álvarez, S. Roldán, C. Blanco, R. Santamaría, M. Granda, and R. Menéndez, *Carbon*, **50**, 828 (2012).
112. C. Flox, J. Rubio-García, M. Skoumal, T. Andreu, and J. R. Morante, *Carbon*, **60**, 280 (2013).
113. X. W. Wu et al., *J. Appl. Electrochem.*, **41**, 1183 (2011).
114. T. Yamamura, N. Watanabe, T. Yano, and Y. Shiokawa, *J. Electrochem. Soc.*, **152**, A830 (2005).
115. P. Chen, M. A. Fryling, and R. L. McCreery, *Anal. Chem.*, **67**, 3115 (1995).
116. M. Gattrell, J. Qian, C. Stewart, P. Graham, and B. MacDougall, *Electrochim. Acta*, **51**, 395 (2005).
117. K. J. Kim, Y. J. Kim, J. H. Kim, and M. S. Park, *Mater. Chem. Phys.*, **131**, 547 (2011).
118. W. Li, J. Liu, and C. Yan, *Electrochim. Acta*, **79**, 102 (2012).
119. S. Zhong and M. Skyllas-Kazacos, *J. Power Sources*, **39**, 1 (1992).
120. D. N. Buckley, *ECS Trans.*, **109**, 3 (2022).
121. M. Al Hajji Safi, A. Bourke, D. N. Buckley, and R. P. Lynch, *ECS Trans.*, **109**, 67 (2022).
122. V. Sasikumar, S. P. R. P. Lynch, M. Al Hajji Safi, D. N. Buckley, and A. Bourke, *ECS Trans.*, **109**, 107 (2022).
123. P. Mazúr et al., *J. Power Sources*, **380**, 105 (2018).
124. M. Becker and T. Turek, *J. Power Sources*, **446**, 227349 (2020).
125. C. Choi, H. Noh, S. Kim, R. Kim, J. H. Lee, J. Heo, and H. T. Kim, *J. Energy Storage*, **21**, 321 (2019).
126. M. Cecchetti, A. Casalegno, and M. Zago, *J. Power Sources*, **400**, 218 (2018).
127. N. Pour, D. G. Kwabi, T. Carney, R. M. Darling, M. L. Perry, and Y. Shao-Horn, *J. Phys. Chem. C Nanomater. Interfaces*, **119**, 5311 (2015).
128. J. O'Donnell, *Next-generation reference electrodes for vanadium flow batteries*. (PhD Thesis, University of Limerick, Ireland) (2020).
129. M. A. Goulet, M. Eikerling, and E. Kjeang, *Electrochem. Commun.*, **57**, 14 (2015).
130. M. Becker, N. Bredemeyer, and N. Tenhumberg, *Electrochim. Acta*, **252**, 12 (2017).
131. D. Dixon et al., *J. Power Sources*, **332**, 240 (2016).
132. Y. Li, J. Parrondo, S. Sankarasubramanian, and V. Ramani, *J. Phys. Chem. C*, **123**, 6370 (2019).
133. S. M. Taylor, A. Pătru, D. Streich, M. El Kazzi, E. Fabbri, and T. J. Schmidt, *Carbon*, **109**, 472 (2016).
134. S. M. Taylor, A. Pătru, E. Fabbri, and T. J. Schmidt, *Electrochem. Commun.*, **75**, 13 (2017).
135. A. Bourke, M. A. Miller, R. P. Lynch, J. S. Wainright, R. F. Savinell, and D. N. Buckley, *ECS Trans.*, **66**, 181 (2015).
136. D. N. Buckley, A. Bourke, R. P. Lynch, N. Quill, M. Miller, J. Wainright, and R. F. Savinell, *MRS Adv.*, **2**, 1131 (2017).
137. D. N. Buckley et al., *ECS Trans.*, **98**, 223 (2020).
138. M. Al-Hajji, *PhD Thesis*, University of Limerick, Ireland (2021).
139. V. A. Garten and D. E. Weiss, *Aust. J. Chem.*, **8**, 68 (1955).
140. L. J. Kepley and A. J. Bard, *Anal. Chem.*, **60**, 1459 (1988).
141. C. Barbero and R. Kötzt, *J. Electrochem. Soc.*, **140**, 1 (1993).
142. M. G. Sullivan et al., *J. Electrochem. Soc.*, **147**, 2636 (2000).
143. M. Al-Hajji-Safi, A. Bourke, D. N. Buckley, and R. P. Lynch, *ECS Trans.*, **77**, 117 (2017).
144. L. Cao, M. Skyllas-Kazacos, and D. W. Wang, *J. Electrochem. Soc.*, **163**, A1164 (2016).
145. J. Noack, N. Roznyatovskaya, J. Kunzendorf, M. Skyllas-Kazacos, C. Menictas, and J. Tübke, *J. Energy Chem.*, **27**, 1341 (2018).
146. S. M. Taylor, A. Pătru, D. Perego, E. Fabbri, and T. J. Schmidt, *ACS Appl. Energy Mater.*, **1**, 1166 (2018).
147. P. Chen and R. L. McCreery, *Anal. Chem.*, **68**, 3958 (1996).
148. T. H. Noh et al., *J. Electrochem. Sci. Technol.*, **8**, 155 (2017).
149. H. Fink, J. Friedl, and U. Stimming, *J. Phys. Chem. C Nanomater. Interfaces*, **120**, 15893 (2016).
150. T. Wu et al., *J. Solid State Electrochem.*, **16**, 579 (2012).
151. Z. He, X. Zhou, Y. Zhang, F. Jiang, and Q. Yu, *J. Electrochem. Soc.*, **166**, A2336 (2019).
152. K. Gass, B. Bera, D. Aaron, and M. M. Mench, *The Electrochem. Soc. Meeting Abstract*, **MA2020-02**, 306 (2020).
153. C. Gao et al., *Electrochim. Acta*, **88**, 193 (2013).
154. J. Liu, S. Liu, Z. He, H. Han, and Y. Chen, *Electrochim. Acta*, **130**, 314 (2014).
155. Z. He, Y. Jiang, W. Meng, F. Jiang, H. Zhou, and Y. Li, *Appl. Surf. Sci.*, **423**, 111 (2017).
156. M. Park, I. Y. Jeon, J. Ryu, J. B. Baek, and J. Cho, *Adv. Energy Mater.*, **5**, 1401550 (2015).
157. I. Derr, M. Bruns, J. Langner, A. Fetyan, J. Melke, and C. Roth, *J. Power Sources*, **325**, 351 (2016).
158. H. Radinger, *ChemPhysChem*, **22**, 2498 (2021).
159. D. M. Hall, R. M. Bachman, and L. R. Radovic, *Carbon Reports*, **1**, 94 (2022).
160. R. M. Bachman, D. M. Hall, and L. R. Radovic, *Carbon*, **201**, 891 (2023).
161. N. Roznyatovskaya, J. Noack, K. Pinkwart, and J. Tübke, *Current Opinion in Electrochemistry*, **19**, 42 (2020).
162. I. Derr et al., *Electrochim. Acta*, **246**, 783 (2017).
163. H. Agarwal, J. Florian, B. R. Goldsmith, and N. Singh, *ACS Energy Lett.*, **4**, 2368 (2019).
164. Z. Jiang and V. Alexandrov, *ACS Appl. Energy Mater.*, **3**, 7543 (2020).
165. X. Z. Yuan, C. Song, A. Platt, N. Zhao, H. Wang, and H. Li, *Int. J. Energy Res.*, **43**, 6599 (2019).
166. A. Bourke, D. N. Buckley, R. P. Lynch, and N. Quill, (2017), Method and system for improving the energy efficiency and for reconditioning of a vanadium flow battery, WO 2017/037239 A1.
167. R. M. Darling and M. L. Perry, (2014), Reactivation of flow battery electrode by exposure to oxidising solution, WO 2014/142968 A1.
168. T. Greese and G. Reichenauer, *J. Power Sources*, **500**, 229958 (2021).
169. L. Wei, X. Z. Fan, H. R. Jiang, K. Liu, M. C. Wu, and T. S. Zhao, *J. Power Sources*, **478**, 228725 (2020).
170. D. Reynard, H. Vrabel, C. R. Dennison, A. Battistel, and H. Girault, *ChemSusChem*, **12**, 1222 (2019).
171. T. Greese, P. A. Loichet Torres, D. Menga, P. Dotzauer, M. Wiener, and G. Reichenauer, *J. Electrochem. Soc.*, **168**, 070554 (2021).
172. C. Sun et al., *Electrochim. Acta*, **318**, 913 (2019).
173. J. Zhang, L. Li, Z. Nie, B. Chen, M. Vijayakumar, S. Kim, W. Wang, B. Schwnezer, J. Liu, and Z. Yang, *J. Appl. Electrochem.*, **41**, 1215 (2011).
174. M. Pourbaix, (1974), Atlas of Electrochemical Equilibria in Aqueous Solutions, National Association of Corrosion Engineers, 2nd English ed.
175. F. T. Silva and T. Ogasawara, *Transactions of the Institution of Mining and Metallurgy, section C, Minerals Processing and Extractive Metallurgy*, **102**, C188 (1993).
176. D. Oboroceanu, N. Quill, C. Lenihan, D. Ní Eidhin, S. P. Albu, R. P. Lynch, and D. N. Buckley, *J. Electrochem. Soc.*, **163**, A2919 (2016).
177. D. Oboroceanu, N. Quill, C. Lenihan, D. Ní Eidhin, S. P. Albu, R. P. Lynch, and D. N. Buckley, *J. Electrochem. Society*, **164**, A2101 (2017).
178. D. Oboroceanu, N. Quill, C. Lenihan, D. Ní Eidhin, S. P. Albu, R. P. Lynch, and D. N. Buckley, *ECS Trans.*, **75**, 49 (2017).
179. D. Oboroceanu, N. Quill, C. Lenihan, D. Ní Eidhin, S. P. Albu, R. P. Lynch, and D. N. Buckley, *MRS Adv.*, **2**, 1177 (2017).
180. D. N. Buckley, D. Oboroceanu, N. Quill, C. Lenihan, D. Ní Eidhin, S. P. Albu, and R. P. Lynch, *J. Electrochem. Society*, **165**, A3263 (2018).
181. D. N. Buckley, D. Oboroceanu, N. Quill, C. Lenihan, D. Ní Eidhin, and R. P. Lynch, *MRS Adv.*, **3**, 3201 (2018).
182. M. Kazacos, M. Cheng, and M. Skyllas-Kazacos, *J. Appl. Electrochem.*, **20**, 463 (1990).

183. M. Skyllas-Kazacos, C. Menictas, and M. Kazacos, *J. Electrochem. Soc.*, **143**, L86 (1996).
184. D. Oboroceanu, N. Quill, C. Lenihan, D. Ní Eithin, S. P. Albu, R. P. Lynch, and D. N. Buckley, *ECS Trans.*, **77**, 107 (2017).
185. D. Oboroceanu, N. Quill, C. Lenihan, R. P. Lynch, and D. N. Buckley, *J. Electrochem. Soc.*, **166**, A2270 (2019).
186. Y. Wen, Y. Xu, J. Cheng, G. Cao, and Y. Yang, *Electrochim. Acta*, **96**, 268 (2013).
187. M. Vijayakumar, L. Li, G. Graff, J. Liu, H. Zhang, Z. Yang, and J. Z. Hu, *J. Power Sources*, **196**, 3669 (2011).
188. M. Skyllas-Kazacos, M. Rychcik, R. G. Robins, A. G. Fane, and M. A. Green, *J. Electrochem. Soc.*, **133**, 1057 (1986).
189. M. Cheng, "Electrolyte optimization and studies for the vanadium redox flow battery." *MSc Thesis University of New South Wales* (1991).
190. M. Vijayakumar, Z. Nie, E. Walter, J. Hu, J. Liu, V. Sprenkle, and W. Wang, *ChemPlusChem*, **80**, 428 (2015).
191. X. Lu, *Electrochim. Acta*, **46**, 4281 (2001).
192. S. Peng, N. Wang, C. Gao, Y. Lei, X. Liang, S. Liu, and Y. Liu, *Int. J. Electrochem. Sci.*, **7**, 4388 (2012).
193. C. Madic, G. M. Begun, R. L. Hahn, J. P. Launay, and W. E. Thiessen, *Inorg. Chem.*, **23**, 469 (1984).
194. J. Livage, *Advanced Zeolite Science and Applications*, ed. J. C. Jansen, M. Stocker, H. G. Karge, and J. Weitkamp (Studies in Surface Science and Catalysis) Vol. 85, p. 1 (1994).
195. G. A. Pozarnsky and A. V. McCormick, *Chem. Mater.*, **6**, 380 (1994).
196. D. N. Buckley, D. Oboroceanu, N. Quill, C. Lenihan, and R. P. Lynch, *J. Electrochem. Soc.*, **168**, 030530 (2021).
197. N. V. Roznyatovskaya et al., *J. Power Sources*, **363**, 234 (2017).
198. L. Cao, M. Skyllas-Kazacos, C. Menictas, and J. Noack, *J. Energy Chemistry*, **27**, 1269 (2018).
199. M. Skyllas-Kazacos and M. Kazacos, *USA Patent*, 6562514 (2003).
200. F. Castellino, S. B. Rasmussen, A. D. Jensen, J. E. Johnsson, and R. Fehrmann, *Appl. Catal. B: Environ.*, **83**, 110 (2008).